Title

Understanding the Decomposition of Dimethyl Methyl Phosphonate on Metal-Modified TiO2(110) Surfaces Using Ensembles of Product Configurations

Journal

ACS Applied Materials & Interfaces, 16(19)

ISSN

1944-8244

Authors

Bonney, Matthew J
Tesvara, Celine
Sautet, Philippe
et al.

Publication Date

2024-05-15

DOI

10.1021/acsami.4c01250

Understanding the Decomposition of Dimethyl Methyl Phosphonate on Metal-Modified TiO_2(110) Surfaces using Ensembles of Product Configurations

Matthew J. Bonney,[1§] Celine Tesvara,[2§] Philippe Sautet,[2,3*] and Michael G. White[1*]

[1]Department of Chemistry, Stony Book University, Stony Brook, NY, USA

[2]Department of Chemical and Biomolecular Engineering, University of California at Los Angeles, Los Angeles, CA, USA

[3]Department of Chemistry and Biochemistry, University of California at Los Angeles, Los Angeles, CA, USA

[§]Co-first authors

*Corresponding authors, sautet@ucla.edu, michael.g.white@stonybrook.edu

Keywords: DMMP, size-selected Cu clusters, TiO_2(110), alkali, NAP-XPS

Abstract

The decomposition of dimethyl methyl phosphonate (DMMP), a simulant for the nerve agent sarin, was investigated on Cu_4/TiO_2(110) and $K/Cu_4/TiO_2$(110) surfaces using a combination of near ambient pressure x-ray photoelectron spectroscopy (NAP-XPS) and density functional theory calculations (DFT). Mass-selected Cu_4 clusters and potassium (K) atoms were deposited onto TiO_2(110) as a metal catalyst and alkali promoter to improve the reactivity and recyclability of the TiO_2 surface after exposure to DMMP. Surface reaction products resulting from decomposition of DMMP were probed by NAP-XPS measurements of the phosphorous (P) 2p and carbon 1s core level spectra. The Cu_4/TiO_2(110) surface is found to be very active for DMMP decomposition, with highly reduced P-species observed even at room temperature (RT). The co-deposition of K atoms and Cu_4 clusters further improves the reactivity with no intact DMMP detectable. Temperature dependent measurements show that the presence of K atoms promotes the

removal of residual P-species at temperatures > 600 K. Detailed DFT calculations were performed to determine the surface structures and energetically accessible pathways on the $Cu_4/TiO_2(110)$ and $K/Cu_4/TiO_2(110)$ surfaces. The calculations show that DMMP and P-containing reaction products preferentially bind to the TiO_2 surface, while the molecular fragments, i.e., methoxy and methyl, bind to both the Cu_4 clusters and TiO_2. The Cu_4 clusters make the P-O, O-C and P-C bond cleavage of DMMP markedly more exothermic. These Cu_4 clusters are highly fluxional, with atomic structures that depend on the configuration of fragments bound to them. Finally, the manifold of P 2p chemical shifts calculated for a large number of energetically favorable configurations of decomposition products is in good agreement with the observed XPS spectra and provides an alternative way of interpreting incompletely resolved core level spectra using an ensemble of observed structures.

I. Introduction

The trapping and decomposition of chemical warfare agents (CWA) is central to the protection of military personnel who may be faced with exposure to CWAs in hostile environments.[1] Some of the most common CWA's are organophosphorus compounds (e.g., sarin, soman, VX) which are readily trapped in high surface area materials, but their complete decomposition and removal as less harmful products under ambient conditions remains a significant challenge.[2-3] Hence, there is a persistent need to develop new materials that can catalyze the decomposition of CWAs and allow regeneration of the active sites under mild conditions.

Much of the literature on the adsorption and initial decomposition of CWA's makes use of the sarin surrogate molecule dimethyl methyl phosphonate (DMMP) which contains the essential chemical and structural characteristics of sarin but with much lower toxicity. The structure of DMMP is shown below

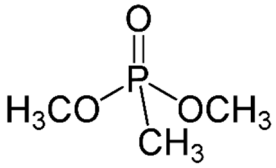

Scheme 1

Due to the strong binding of DMMP to metal oxide materials, there is currently a large literature base that has explored the binding and decomposition pathways of DMMP on numerous bulk oxides (e.g., Al_2O_3, TiO_2, MoO_2, Fe_2O_3, Cu_2O), mixed oxides (e.g., V_2O_5/Al_2O_3) and porous oxides materials such as metal organic frameworks (MOFs) and polyoxometalates (POMs).[3-8] Many of these oxide materials have been shown to be effective for the initial stages of DMMP decomposition in which methoxy and methyl groups are sequentially removed by interactions with Lewis acidic centers on the oxide surface, while P is stabilized by interaction with surface O atoms. These reactions can lead to the formation of gas-phase products, e.g., methanol, CO_2, CO, CH_4 (depending on the catalyst), and the formation of methyl phosphonic acid or phosphates which

remain on the surface. The latter are strongly bound to the metal cations of the oxide and are not easily removed except at very high temperatures (> 700 K for TiO_2).[9-11] Hence, the surface bound phosphate derivatives act to poison the surface and prevent subsequent DMMP adsorption and reaction.

Adding an active transition metal (TM) to the oxide surface as a supported nanoparticle (NP, e.g., Pt, Au, Cu, Ni) enhances DMMP adsorption and reaction. The enhanced reactivity appears to result from increasing the reducibility of the oxide as well as DMMP adsorption/reaction on the metals themselves; however, the higher activity of systems such as Pt/TiO_2 or Ni/TiO_2 also results in a larger amount of residual PO_x on the surface that is more resistant to removal.[11-16] More recent studies of single metal atoms supported on the metal oxide nodes of metal organic frameworks (MOFs), e.g., Cu@MOF-UiO-66, suggest that the isolated metal cation can be active for promoting DMMP decomposition, while also blocking the bridged binding site for phosphate decomposition products on the zirconia node. Unlike larger Cu NPs which are metallic, the single Cu atoms incorporated into the MOF were found to be cationic, Cu(I) and Cu(II), with the distribution of oxidation states dependent on pretreatment. Theoretical studies on the Cu@UiO-66 system show that the weaker Lewis strength of the Cu cations and the blocking of zirconia node sites should result in overall better performance than the pristine MOFs.

In this work, we explored the decomposition of DMMP on size-selected Cu_4 clusters supported on $TiO_2(110)$ with and without the presence of an alkali metal modifier, i.e., K atoms. This combination of materials adopts many modifications expected to improve CWA decomposition and catalyst regeneration by decreasing the metal particle size to promote the formation of cationic Cu atoms via direct interaction with the titania support; (2) use of a reducible oxide, TiO_2, to allow the formation Ti^{3+} cations with lower Lewis strength via O-vacancy

formation; (3) adding an alkali modifier (K) to further increase the basicity of the oxide support to weaken DMMP interactions. Periodic DFT calculations predict a tetrahedral or rhombus-like structure for the Cu_4 cluster on $TiO_2(110)$ in which the cluster is anchored by 2-3 Cu-O bonds.[17-20] Bader charge analyses show that the Cu atoms bonding to surface O-atoms donate electrons to the surface, while those directed away from the surface are largely unaffected, leading to an overall charge of +1.5 to +1.9 on the cluster.[18,20] These calculations suggest that cationic $Cu^{\delta+}$ species, which were implicated as favorable for DMMP decomposition on copper oxide surfaces, are accessible on $Cu_4/TiO_2(110)$.[21-23] As a reducible oxide, TiO_2 alone or as support for metals (Cu, Ni, Pt, Au) has been widely studied for the decomposition of CWA's and simulants, but the presence of O-vacancies or participation of associated lattice O-atoms is generally not evident except at elevated temperatures where vacancy formation becomes favorable (> 450 K). [3,9,11-13,15-16,24-28] In the case of rutile $TiO_2(110)$, a recent theoretical study showed that reduced Ti^{3+} cations at O-vacancies act as adsorption sites for DMMP, but with a slightly lower adsorption energy compared with the pristine surface, consistent with the lower cation acidity.[29] Oxygen vacancies are shown to play an important role in reducing the barrier for P-OCH_3 cleavage, but the barrier values remain rather high and decomposition is unlikely below ~600 K consistent with experiments on bare $TiO_2(110)$.[26,29] In this work, we co-deposit an alkali atom, K, to enhance the basicity and reducibility of the TiO_2 support via electron transfer, e.g., $K + Ti^{4+} \rightarrow K^{+} + Ti^{3+}$.[30-34] The increased basicity of the surface is expected to weaken the strength of the P-O-$Ti^{3+/4+}$ bonds, making it easier to remove the final PO_x decomposition products.[35-36] Alkali addition has also been shown to increase Pt and Au dispersion to very small clusters on TiO_2, even single atoms, while also improving the activity of Au or Cu/TiO_2 catalysts for oxidation reactions, i.e., CO oxidation and the water-gas-shift reaction.[37-43]

Surfaces of $Cu_4/TiO_2(110)$ and $K/Cu_4/TiO_2(110)$, noted hereafter as Cu and K-Cu, respectively, were tested for reactivity with DMMP using near ambient pressure XPS at a pressure of $1x10^{-4}$ Torr of DMMP. The P 2p and C 1s core level spectra were used to identify surface intermediates resulting from adsorption and decomposition of DMMP and their stabilities on the surfaces from room temperature to 800 K. The Cu and K-Cu surfaces are found to be remarkably active for DMMP decomposition, with highly reduced P-species observed even at room temperature. To explain these results, detailed ab initio DFT calculations were performed to determine the structures of the Cu and K-Cu surfaces and elucidate the complex decomposition pathways that involve synergistic interactions between Cu_4, K and the TiO_2 surface. The calculations show that the Cu_4 clusters strongly promote P-O, O-C and P-C bond cleavage of DMMP by stabilizing the products of these decomposition and are highly fluxional with atomic structures that depend on the configuration of fragments bound to the surface. Moreover, the large number of energetically accessible configurations of decomposition products results in a near continuous distribution of calculated P 2p chemical shifts that proposes an alternative approach to assigning broad, unresolved core level spectra.

II. Methods

II.A Experiments

The Cu and K-Cu surfaces were prepared in a home-built mass-selected cluster deposition instrument described in more detail elsewhere. Briefly, a magnetron sputtering source (Oxford Applied Research, NC200U-B) using a Cu target was used to generate Cu_4^+ cluster ions which were mass-selected by quadrupole mass filter prior to deposition onto a clean $TiO_2(110)$ single crystal in UHV conditions. Neutral clusters were removed by deflecting the ion beam through an electrostatic bender located upstream of the quadrupole filter. The number of deposited clusters

ions was determined from the integrated ion current on the sample during deposition as measured by a picoammeter. For both Cu and K-Cu surfaces, $3x10^{13}$ cluster ions were deposited onto the $TiO_2(111)$ support in a ~5 mm diameter spot, corresponding to an average coverage of ~0.07 ML. Potassium atoms were evaporated onto one of the $Cu_4/TiO_2(110)$ samples using an electrochemical getter source (SAES) using previously determined deposition conditions.

The $TiO_2(110)$ single crystals (CrysTec; 10 x 10 mm^2, 1 mm thick) were mounted onto a molybdenum flag-style sample plates and cleaned by multiple cycles of Ar^+ ion sputtering at 1 keV for 30 min followed by annealing at 800 K for 30 min. These cleaning cycles are repeated until the $TiO_2(111)$ was bulk reduced as evidenced by a color change to a dark shade of blue. The surfaces were then oxidized by exposure to $1x10^{-6}$ Torr of O_2 at 800K for 30 min and slowly cooled to RT, in order to heal bridged-oxygen atom vacancies resulting from sputtering and annealing.[33,44-46] Following these treatments, XPS measurements confirmed that the $TiO_2(110)$ surfaces were free of contamination and mostly "oxidized" with very small contributions from reduced Ti^{3+} cations (< 2%) in the Ti 2p spectra.

After preparation and in-house characterization by XPS, the prepared Cu and K-Cu samples were transferred to a vacuum suitcase, and then transported and loaded into a NAP-XPS instrument located at the Center for Functional Nanomaterials at Brookhaven National Laboratory. The vacuum suitcase uses a small getter pump (Z100 model, SAES Getters) to maintain UHV pressures (10^{-9} Torr). The NAP-XPS instrument consists of a Specs PHOIBOS 150 NAP differentially pumped hemispherical analyzer and electrostatic lens system. The photon source is a monochromatized and focused x-ray source (Al Kα, 1486.6 eV; 300 μm spot size). The Cu or K-Cu samples were loaded onto a four-axis manipulator (xyz-ϕ) where the crystal face could be positioned close (600 μm) to the differential pumping cone (300 μm dia) of the XPS analyzer to

maximize signal. The manipulator was also used to translate the sample under the XPS entrance cone in order to obtain spatially resolved core level spectra at different points on the sample with different coverages of Cu_4 clusters.

NAP-XPS measurements for DMMP decomposition on the Cu and K-Cu surfaces were taken with a background pressure of 1 x 10^{-4} Torr of DMMP at RT. The DMMP was introduced into the analysis chamber via a precision leak valve. After the RT measurements, the DMMP was evacuated to restore the analysis chamber to high vacuum (~1 x 10^{-8} Torr) and XPS measurements were taken at elevated temperatures between 400 K and 900 K. The sample temperature was measured via a type-K thermocouple attached to the sample plate. The DMMP liquid sample was thoroughly degassed prior to use via repeated freeze-and-thaw cycles using liquid nitrogen. Core level spectra for Cu 2p, Ti 2p, O 1s, C 1s, K 2p, P 2p and Cu $L_3M_{4,5}M_{4,5}$ (simplified as LMM) Auger were collected with a 20 eV pass energy. The resulting spectra were least-squares fitted with Shirley background contributions using CasaXPS software. The Ti^{4+} $2p_{3/2}$ binding energy of 458.8eV for the TiO_2(110) substrate was used to calibrate the energy spectra.[47]

The NAP-XPS instrument samples a very small area on the samples (300μ dia. spot) and the local coverage of Cu_4 and K for the spots probed in this work were estimated from the measured XPS total intensities for the Ti 2p, Cu 2p and K 2p core levels and published photoionization sensitivity factors.[48] From the relative Cu:Ti XPS signals, the coverage of Cu_4 clusters on the Cu and K-Cu surfaces were estimated to be ~0.05 ML, which is close to the 0.07 ML expected from the integrated ion current. The K coverage for the same spot on the K-Cu surface is 0.06 ML, while for the K/TiO_2(110) surface, the K coverage at the measured spot was roughly half at 0.03 ML.

II.B Theory

The density functional theory (DFT) calculations in this study were performed using the Vienna Ab initio Simulation Package (VASP). The Perdew-Burke-Ernzerhof (PBE) functional was employed, along with a Hubbard U correction of 4.2 eV applied to Ti sites to better describe the onsite coulomb repulsion of the Ti 3d orbitals. This particular U value of 4.2 eV was chosen to accurately represent the electronic structure observed experimentally in TiO_2, particularly in relation to the localized nature of electrons on surfaces with oxygen vacancies. The dDsC dispersion correction was implemented to account for long-range van der Waals interactions. The one electron orbitals are developed on a bais set of plane waves, with a cutoff energy set at 500 eV and the convergence criterion were established at 10^{-6} eV for electronic energies and within 0.03 eV/Å for atomic forces. To correct for the spurious dipole-dipole interaction between neighboring slabs in the z-direction, the Harris correction (Makov-Payne) was applied. Transition states were determined using the Nudged Elastic Band Method with eight intermediate images, with climbing image turned on after the forces of all images are below 0.1 eV.

The adsorption energies and reaction pathway energies for systems with Cu_4 and Cu_4K were calculated using Equation 1 and 2 respectively:

$$E_{DMMP_{ads}} = E_{intermediate} - E_{TiO2+Cu_{cluster}} - E_{DMMP}$$

$$E_{DMMP_{ads}} = E_{intermediate} - E_{TiO2+Cu_{cluster}+K} - E_{DMMP}$$

The 2x5 TiO_2(110) surface was built from the bulk crystal structure. The bulk lattice constants were computed with a gamma-centered k-points mesh of 4x4x4, resulting in values of a = 4.65 Å and c = 3.02 Å. The 2x5 surface lattice vectors were determined from the bulk geometry as a = 13.16 Å and b = 15.09 Å. This surface comprised four O-Ti-O trilayers, equivalent to 12 atomic layers. A vacuum distance of 15 Å was introduced between slabs to prevent periodic

interactions along the z-direction. The bottom three atomic layers were kept frozen to emulate the bulk. All surface calculations employed a k-point mesh of 1x1x1. Using a larger k-points mesh (e.g., 3x3x1) or thicker surface models did not yield significant differences compared to our selected 2x5 surface, calculated at the gamma point.

A total of 22 and 25 isomers of deposited Cu_4 clusters and Cu_4 clusters with K atoms were manually generated and explored exhaustively. The stabilities of each isomer are expressed relative to the most stable one. Subsequently 290 isomers of molecular and dissociative DMMP adsorption were explored on the Cu_4/TiO_2 and $K/Cu_4/TiO_2(110)$ surfaces.

III. Results

III.A Experimental characterization of $Cu_4/TiO_2(110)$ and $K/Cu_4/TiO_2(110)$

Figure 1 provides a summary of the state of the Cu and K-Cu surfaces prior to DMMP exposure. The level of reduction of the $TiO_2(110)$ support was inferred from Ti 2p XPS spectra that were fitted to contributions from Ti^{4+} and reduced Ti^{3+} cations that appear at lower binding energies. Figures 1a and 1d show that the $TiO_2(110)$ surface is only slightly reduced for both the as-prepared Cu (3.8% Ti^{3+}) and K-Cu (7.5% Ti^{3+}) surfaces; adding K increases surface reduction by about 60% as expected for electron transfer to the TiO_2 support (Fig. 1d). The Cu 2p spectrum in Fig. 1b is characteristic of both surfaces with the binding energies consistent with Cu^0 and/or Cu^{1+} as these oxidation states typically are too close to be resolved. Moreover, the K 2p binding energies are consistent with completely ionized to K^+ when deposited onto oxide surfaces (Fig. 1e).[39,49] The Cu LMM Auger spectra are complicated by overlap with the Ti 2s core level and associated satellites, but the satellite peak at ~577.4 eV is largely free of overlaps and was used to fix the Ti 2s contributions for the entire spectrum. The relative intensities and peak widths for the

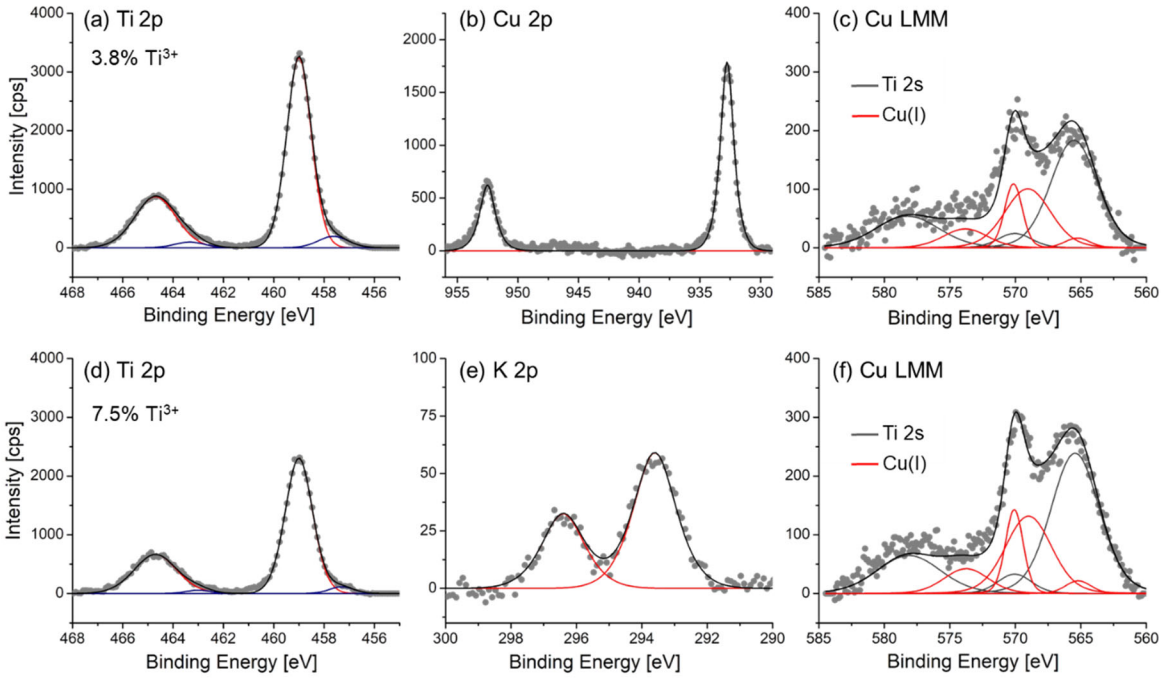

Figure 1: Surface characterization using Ti 2p (a, d) , Cu 2p (b, e), and K 2p (c, f) XPS spectra and Cu LMM Auger spectra prior to DMMP exposure for the (a) $Cu_4/TiO_2(110)$ and (b) $K/Cu_4/TiO_2(110)$ surfaces.

Ti 2s states were experimentally determined from the bare $TiO_2(110)$ surface. The least-squares fits included LMM contributions from both Cu^0 and Cu^{1+} along with the scaled Ti 2s peaks, but the Cu^0 contribution was found to be too small to fit with confidence (see SI for description of fitting).[50] The sharp peak near 570.1 eV (kinetic energy of 916.6 eV) is a signature of Cu^{1+} whereas Cu^0 has a characteristic peak near 568.3 eV (kinetic energy of 918.4).). As shown in SI, significant Cu^0 contributions are only observed for LMM Auger spectra taken after exposure to DMMP and heating to 900 K (Figure S1). Hence, the fits shown in Figures 1c and 1f only include contributions from Cu^{1+} LMM and the Ti 2s photoemission peaks; these spectra indicate that Cu^{1+} is the dominant oxidation state in the Cu_4 clusters on the as-prepared Cu and K-Cu surfaces.

III.B Theoretical description of $Cu_4/TiO_2(110)$ and $K/Cu_4/TiO_2(110)$ surfaces and adsorption of molecular DMMP

The calculated lowest energy structures of the Cu and K-Cu surfaces are shown in Figure 2. The Cu_4 cluster on TiO_2(110) maximizes the interaction with the surface by adopting monolayer structures, either as flat rhombus or square geometries, while the tetrahedral structure lies +0.64 eV higher in energy (Fig. 2, top row). The Cu atoms interact with bridging O atoms of the TiO_2(110) surface. These structures are similar to those found in previous DFT calculations of Cu_4 clusters on TiO_2(110).[17-20] From the Bader charge analyses shown in Figure 3, the Cu_4 cluster donates 0.84e to the surface for the most stable configuration, which results in spin density localization observed on the two Ti atoms located below the Cu_4 cluster (with values ~1 and 0.1 μB, Figure 3a).

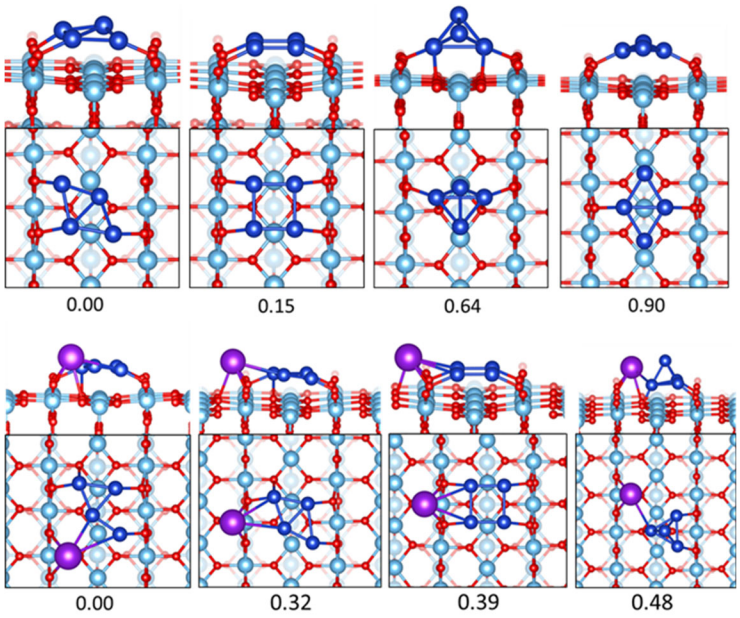

Figure 2: Side and top views of the lowest energy structures for Cu_4/TiO_2(110) and $K/Cu_4/TiO_2$(110). Values below each structure denote the relative stabilities (in eV) with respect to the most stable structures shown on the left. Atom colors: Ti: light blue; O: red; Cu: dark blue; K: purple.

The optimized structures for the K-Cu surface (Fig. 2, bottom row) show that the K atom binds to the TiO_2 surface but is located next to the Cu_4 cluster, inducing a deformation of the cluster geometry. The latter suggest a preference for forming a K-Cu_4 interface, but may also reflect the limited unit cell size (5x2) which could restrict the maximum separation of the Cu and K species. To further clarify this point, we have added a new figure in SI, Figure S3, which shows

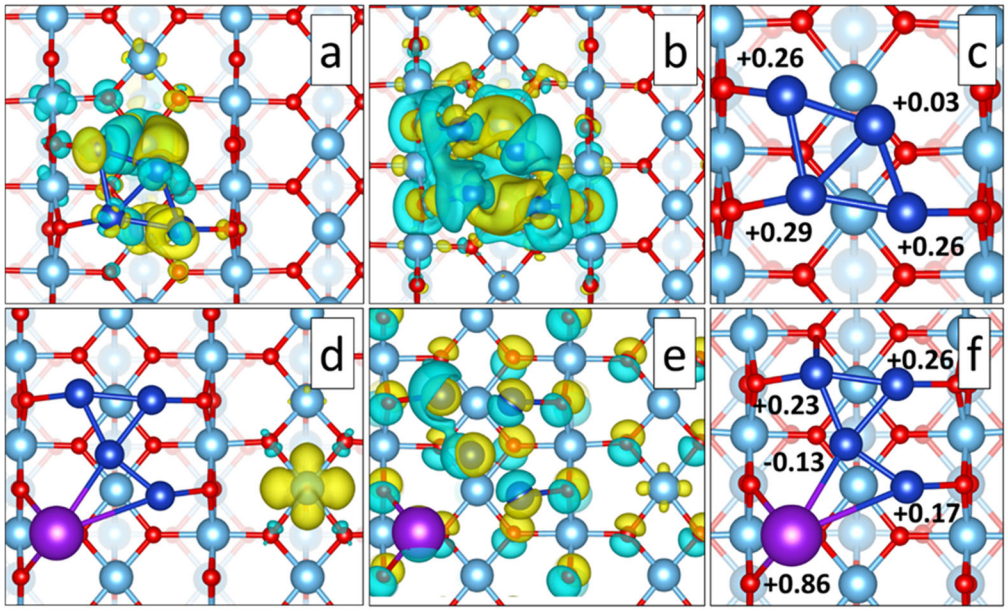

Figure 3: (a, d) Electronic spin density for the most stable (a) $Cu_4/TiO_2(110)$ and (d) $K/Cu_4/TiO_2(110)$ structures; (b, e) charge density difference upon adsorption of (b) Cu_4 and (e) $K\text{-}Cu_4$ adsorption on $TiO_2(110)$. The yellow and blue color denotes spin up and down density or charge accumulation and depletion, respectively. (c, f) Electronic Bader charge for (c) Cu_4 and (f) K/Cu_4 on $TiO_2(110)$. Atom colors: Ti: light blue; O: red; Cu: dark blue; K: purple.

a larger number of calculated K-Cu structures. The lowest energy structure has the K atom attached to the TiO_2 surface, but located next to the Cu_4 cluster with direct interactions with two of the Cu atoms. By comparison, a configuration in which the K atom and Cu_4 cluster are located too far apart to interact is +0.55 eV less stable. These calculations suggest that the addition of K atoms modifies the surface via direct interactions with both the support and metal cluster. Electronic interactions are evident in the Bader charges resulting from electron donation from the K atom (Fig. 3d-f). Here, the K atom is completely ionized, creating a localized electron on a nearby Ti_{5c} atom (spin 1 μB, Fig. 3d). Interactions with the K atom also modify the Bader charges on the Cu atoms within the Cu_4 cluster and reduce its overall charge donation to the TiO_2 (~0.5e) surface compared to the Cu-only surface (~0.8e). Nonetheless, the calculations for both the Cu and K-Cu

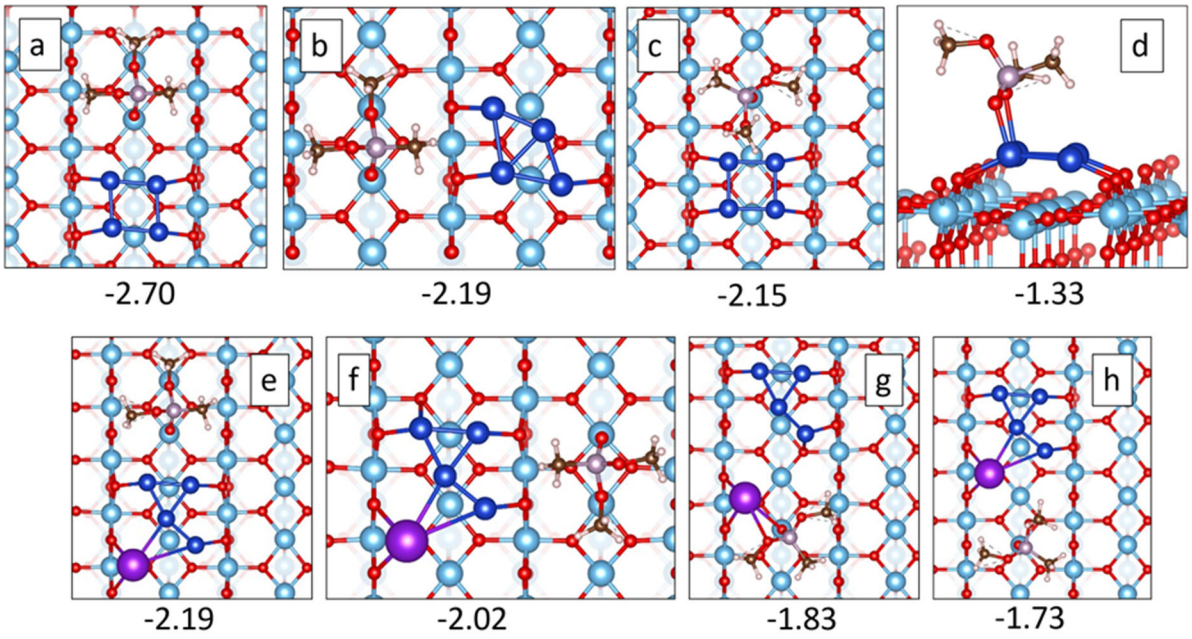

Figure 4: Low energy surface configurations for DMMP adsorption on (a-d) $Cu_4/TiO_2(110)$ and (e-h) $K/Cu_4/TiO_2(110)$. DMMP adsorption energies are shown below each figure (in eV). Atom colors: Ti: light blue; O: red; Cu: dark blue; K: purple; P: silver; C; brown.

surface suggest the presence of cationic $Cu^{\delta+}$ atoms on surfaces, which is in qualitative agreement with the observed Cu LMM Auger spectra (Fig.s 1c ad 1f).

The calculated lowest energy structures for binding molecular DMMP on the Cu and K-Cu surfaces are shown in Figure 4. DMMP prefers to bind to the $TiO_2(110)$ surface and not onto the Cu_4 cluster or K atom. For the lowest energy configurations (Fig.s 4a and 4e), DMMP binds in an η_2-O-P-O(CH_3) configuration to two Ti_{5c}^{4+} cations aligned along the [001] direction of the $TiO_2(110)$ surface, while the second methoxy and the methyl groups are oriented along the perpendicular $[1\bar{1}0]$ direction. This DMMP adsorption structure is essentially identical to that calculated for DMMP on the bare $TiO_2(110)$ surface.[29,51] On the Cu surface (Fig. 4a), the Cu_4 cluster is located in the same row as DMMP and adopts a square geometry by forming four Cu-O bonds with nearby bridging O-atoms. This is also the case on the K-Cu surface (Fig 4e) although the structure of the Cu_4 cluster is modified by direct interactions with the K atom. For the other

low lying isomer configurations, DMMP remains mostly bonded to the TiO_2(110) surface, but can also interact with the Cu_4 cluster (Fig. 4c) or K atom (Fig. 4g).

Although the lowest energy adsorption structures for DMMP on the Cu, K-Cu and bare TiO_2(110) surfaces are essentially the same, the DMMP adsorption energies show that addition of the Cu_4 cluster strengthens DMMP binding (-2.70 eV), while K addition destabilizes DMMP binding (-2.19 eV) relative to DMMP on the bare TiO_2 (110) surface (-2.35 eV). The latter value was recently reported by Tesvara, et al., using a similar level of DFT.[29,51] The lower DMMP adsorption energy on the K-Cu surface is attributed to the additional electron charge donated from the K atoms to the TiO_2 surface as indicated by the calculated Bader charges (Fig.s 3c and 3f). Lowering the binding energies of DMMP and its decomposition fragments is one of the expected outcomes of alkali addition, as electron transfer to the TiO_2 surface should effectively decrease the Lewis acidity of the Ti_{5c} cations and weaken bonds to electrophilic adsorbates like DMMP.

III.C NAP-XPS results for DMMP exposure at room temperature

The P 2p spectra shown in Figure 5 for the Cu and K-Cu surfaces exposed to DMMP at RT consist of a number of overlapped peaks that extend over a range of ~8 eV. The spectrum for the Cu only surface (Fig. 5a) could be fit to four P 2p doublets (labeled P_1-P_4) where the peak widths and doublet separations (0.85 eV) were constrained to be the similar.[52] For the K-Cu surface (Fig. 5b), the spectrum starts at lower binding energy and requires only three P 2p doublets to fit the data, with binding energies essentially the same as peaks P_2-P_4 in the Cu spectrum. By comparison, the K only surface exhibits only one P 2p peak (Figure 5c), with a fitted binding energy identical to peak P_1 in the Cu only spectrum. We note that the K only spectrum was obtained by moving the small NAP-XPS entrance aperture (300 μm) to the edge of the K-Cu surface where

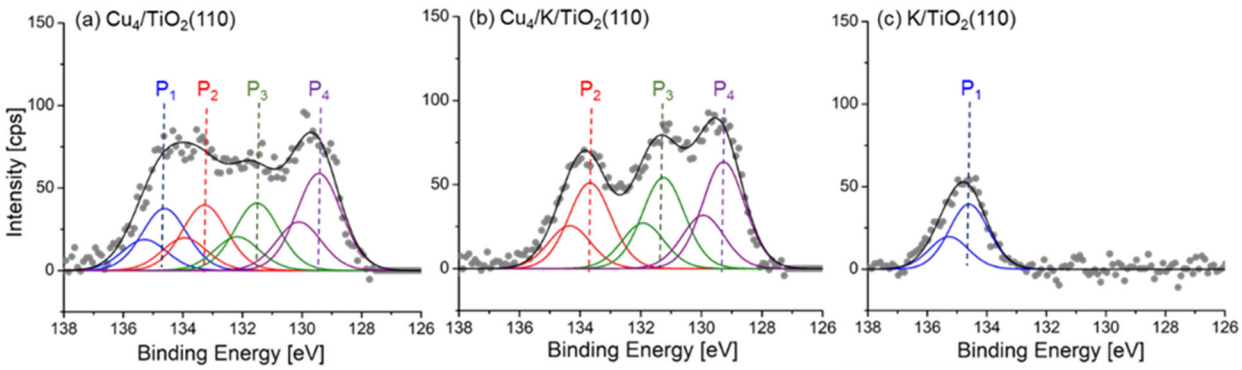

Figure 5: P 2p XPS spectra showing phosphorous surface species during exposure of $1x10^{-4}$ Torr of DMMP at room temperature on the surfaces of (a) Cu_4/TiO_2, (b) $K/Cu_4/TiO_2(110)$ and (c) $K/TiO_2(110)$.The different colored solid lines correspond to least-squares fits of the data to four different P 2p doublets labeled P_1-P_4.

there was no detectable Cu; the Cu_4 cluster deposition area was limited to region 3-4 mm (dia) near the center of the $TiO_2(110)$ substrate.

The binding energies for the best-fit P $2p_{3/2}$ peaks for all three surfaces are given in Table 1 along with those obtained on related surfaces reported in the literature. The $2p_{3/2}$ binding energy for P_1 (134.6 eV) is similar to chemisorbed DMMP on bare $TiO_2(110)$,[26] Ni and Pt nanoparticles (NPs) supported on $TiO_2(110)$[11,53] and bulk Cu_2O[22] and CuO[21] surfaces. Additional support for assigning P_1 to chemisorbed DMMP comes from P 2p XPS spectra which show that P_1 disappears from the Cu surface at ~500 K (see Figures 7a and S5b in SI). On $TiO_2(110)$ surfaces with and without metals, chemisorbed DMMP was shown to desorb reversibly and/or decompose at temperatures > 400 K.[11-12,16,26] Hence, we assign P_1 to intact, chemisorbed DMMP. As P_1 is the only peak observed on the K-only surface (Fig. 5c), we conclude that the K-only surface is unreactive with respect to DMMP at RT, similar to bare $TiO_2(110)$.[26,29] Moreover, the fact that P_1

Table 1: Summary of P 2p and C 1s binding energies for DMMP on TiO_2(110) surfaces with and without Cu_4 clusters and K atoms, along with data from previous studies on related surfaces.

Surface	P_1	P_2	P_3	P_4	C_1	C_2	C_3
$K/Cu_4/TiO_2$	----	133.6	131.2	129.2	288.8	287.0	285.5
Cu_4/TiO_2	134.6	133.3	131.5	129.4	288.9	287.2	285.4
K/TiO_2	134.6	n/a	--	--	288.7	287.3	285.8
TiO_2[a]	134.9[g]	--	--	-	--	287.7[n]	286.3[o]
Cu-NP/TiO_2[b]	134.9[g]	133.7[h]	--	-	--	287.7[n]	286.3[o]
Ni-NP/TiO_2[c]	134.5[g]	133.7[h]	--	129.1[l]	--	287.8[n]	286.3[o]
Pt-NP/TiO_2[d]	134.8[g]	134.0[h]	--	129.5[l]	--	287.8[n]	286.3[o] 284.6[p]
CuO[e]	133.8[g]	132.8[i]	---	--	288.1[m]	287.1[n]	285.1[o]
Cu_2O[f]	134.1[g]	133.1[i]	132.1[j] 130.0[k]	128.9[l]	--	286.4[n]	284.2[o]

[a] Ref [26] UHV dose at RT
[b] Ref [12] UHV dose at RT
[c] Ref [16] UHV dose at RT
[d] Ref [11] UHV dose at RT
[e] Ref [21] exposure to $1x10^{-4}$ Torr DMMP at RT
[f] Ref [22] exposure to $1x10^{-4}$ Torr DMMP at RT
[g] Chemisorbed DMMP
[h] PO_x
[i] Methyl methyl phosphonate (MMP) $O=P(OCH_3)(CH_3)O$
[j] Phosphinate, $O=PH(OCH_3)O$-Cu
[k] Phosphine, Cu-P-CH_3 or O-P-CH_3
[l] Atomic phosphorous, P-Cu or P-O
[m] carbonate, CO_3^{2-}
[n] methoxy, -OCH_3
[o] P-CH_3
[p] Pt-CH_x

does not appear in the P 2p spectrum for the K-Cu surface (Fig. 5b) indicates that intact DMMP is not stable on this surface at RT and is thereby more reactive than the Cu or K-only surfaces.

The P_2-P_4 peaks appearing at lower binding energies are assigned to the decomposition products of DMMP in line with previous studies. In particular, the P 2p spectra for the Cu and K-Cu surfaces are similar to those obtained for DMMP exposure on a polycrystalline Cu_2O surface using NAP-XPS under identical conditions, i.e., RT and $1x10^{-4}$ Torr of DMMP.[22] On the Cu_2O surface, the P 2p peaks from highest to lowest binding energies were assigned to chemisorbed DMMP, methyl methylphosphonate (MMP), phosphinate, phosphine ($P\text{-}CH_3$) and atomic phosphorous (P).[22] These assignments indicate that the degree of DMMP fragmentation and P-atom reduction increases with decreasing P 2p binding energy. Although the P 2p binding energies for the Cu_2O surface differ somewhat from those observed here (see Table 1), we can tentatively and initially assign the P_2 peaks to MMP and P_4 to atomic-P, while the P_3 peak results from unresolved contributions from other species such as phosphinate and phosphine. These assignments will be later reanalyzed in the light of the theory simulations. The assignments for P_2 (MMP) and P_4 (atomic P) are consistent with those proposed for Ni and Pt NPs supported on TiO_2(110), and both are observed at temperatures ≥ 400 K, while only P_4 is present after heating to 850 K.[11,53] In sharp contrast to the results presented here, larger Cu nanoparticles (4-15 nm) supported on TiO_2(110) were reported to be mostly unreactive towards DMMP at saturation coverage, with only the P_2 species present at RT and a very small contribution from P_4 after heating to > 700 K.[12] Although the DMMP exposure conditions were very different in the latter work, the results presented here (Fig. 5) strongly suggest that the small Cu_4 clusters with and without co-deposition of K are far more reactive than larger Cu nanoparticles on the same support, TiO_2(110).

The C 1s core level spectra for the Cu and K-Cu surfaces taken under 1 x 10^{-4} Torr of DMMP at RT are shown in Figure 6. These spectra were obtained by subtracting the background spectra taken under high vacuum conditions prior to DMMP exposure (see Figure S4). This

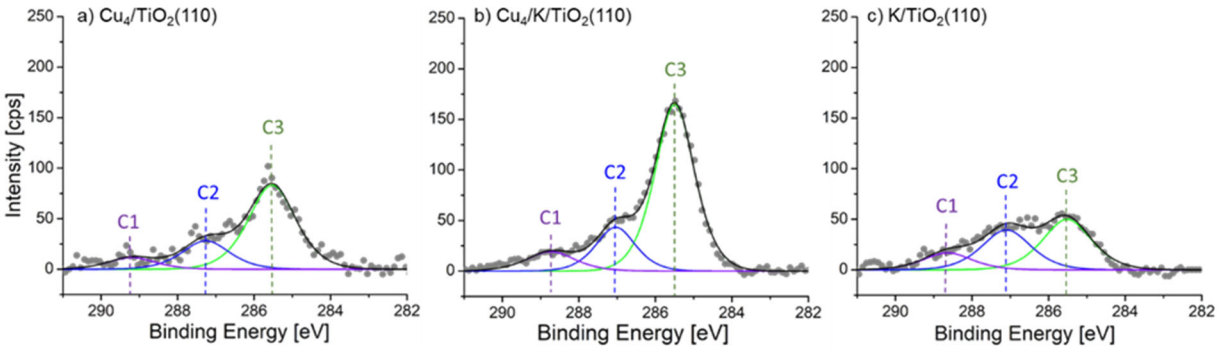

Figure 6: C1s XPS spectra taken on the (a) $Cu_4/TiO_2(110)$, (b) $K/Cu_4/TiO_2(110)$ and (c) $K/TiO_2(110)$ surfaces under $1x10^{-4}$ Torr of DMMP at room temperature. The colored solid lines correspond to least squares fits of the data to three different peaks corresponding to different surface intermediates with labels C_1-C_3.

eliminates contributions from adventitious carbon (C_{ad}) and other species resulting from the decomposition of background gases during the transfer and exchange of samples in the NAP-XPS instrument. The resulting spectra could be least-squares fit with three peaks, C_1-C_3, with similar, but not identical binding energies on all three surfaces. The fitted C 1s binding energies are given in Table 1. Earlier studies of DMMP on bare $TiO_2(110)$[26] and metal NP's (NPs; Cu, Ni, Pt) supported on $TiO_2(110)$[11-12,53] found C 1s peaks with binding energies very close to that observed here for C_2 and C_3; the latter were assigned to methoxy ($*OCH_3$) and methyl ($*CH_3$), respectively. As shown in the calculations described later, both methoxy and methyl can be bound to the P-atom in DMMP or DMMP fragments, and as dissociation products bound to the Cu_4 clusters or Ti^{4+} cations on the TiO_2 surface. The higher binding energy for the C_1 peak is in the range for formate (HCOO*) and carbonate (CO_3*) which have been observed in IR spectra of titania supported powder systems exposed to ambient pressures of DMMP.[24,28] Here we will identify C_1 as an oxidized carbon species, CO_x. The fraction of CO_x is small compared to the other carbon intermediates on the all three surfaces (10-20%).

For the bare TiO_2(110) surface and larger Cu NPs on TiO_2(111) surface at RT, Ma et al., measured the methoxy-to-methyl (C_2:C_3) peak ratio to be approximately 2:1 suggesting the presence of only intact molecular DMMP (see Scheme 1).[12,26] Ratios ≤ 1 are typical for surfaces on which DMMP decomposes via P-OCH_3, PO-CH_3 or P-CH_3 bond cleavage. For the Cu only surface studied here, the methoxy-to-methyl ratio is 0.34 and is even smaller for the K-Cu surface, 0.26. The smaller value for K-Cu is consistent with the earlier conclusion that no molecular DMMP is present on this surface. The observed C2:C3 ratios suggest that DMMP decomposition on the Cu and K-Cu surfaces leads to a build-up of methyl fragments on the surface that could result from preferential P-CH_3 and PO-CH_3 bond cleavage of DMMP or other P-intermediates. Methoxy fragments could also be lost via secondary reactions, e.g., methanol formation followed by desorption, but this is less likely at RT. For the K-only surface (Fig. 6c), the ratio is C_2:C_3 ratio is larger than for Cu and K-Cu but is still less than one (0.78), which is unexpected since the P 2p spectrum suggests the presence of only unreacted DMMP on the surface (Fig. 5c). We tentatively attribute the K-only spectrum to spillover of C-based fragments from the center of the sample, where the Cu_4 clusters are deposited, to the edges of the support where only K is present. Hence, the K-only C 1s spectrum is a likely a combination of chemisorbed DMMP and C fragments generated from the K-Cu regions (center) of the surface. Overall, the results in Figure 6 indicate that DMMP decomposition leads to a larger fraction of methyl products on the K-Cu and Cu surfaces. Moreover, the K-Cu surface is significantly more reactive as evidenced by the larger surface concentration of carbon-based intermediates (~1.8 times more than Cu only surface).

As shown in Figure S2 in SI, the Cu LMM Auger spectra for the Cu and K-Cu surfaces during exposure of $1x10^{-4}$ Torr of DMMP at RT are nearly identical to the surfaces prior to DMMP

exposure (see Fig. 1c and 1f). These results show that DMMP adsorption and decomposition do not alter the Cu oxidation state, which remains mostly Cu^{1+} in the Cu_4 clusters at RT.

III.D Temperature dependence

Figure 7 shows the temperature dependence of the P-based and C-based surface species on the Cu and K-Cu surfaces following DMMP exposure at RT. Heating experiments were performed under high vacuum (~$1x10^{-8}$ Torr) after DMMP was pumped out of the XPS main chamber. The individual P 2p and C 1s XPS spectra at each temperature from which these curves were derived

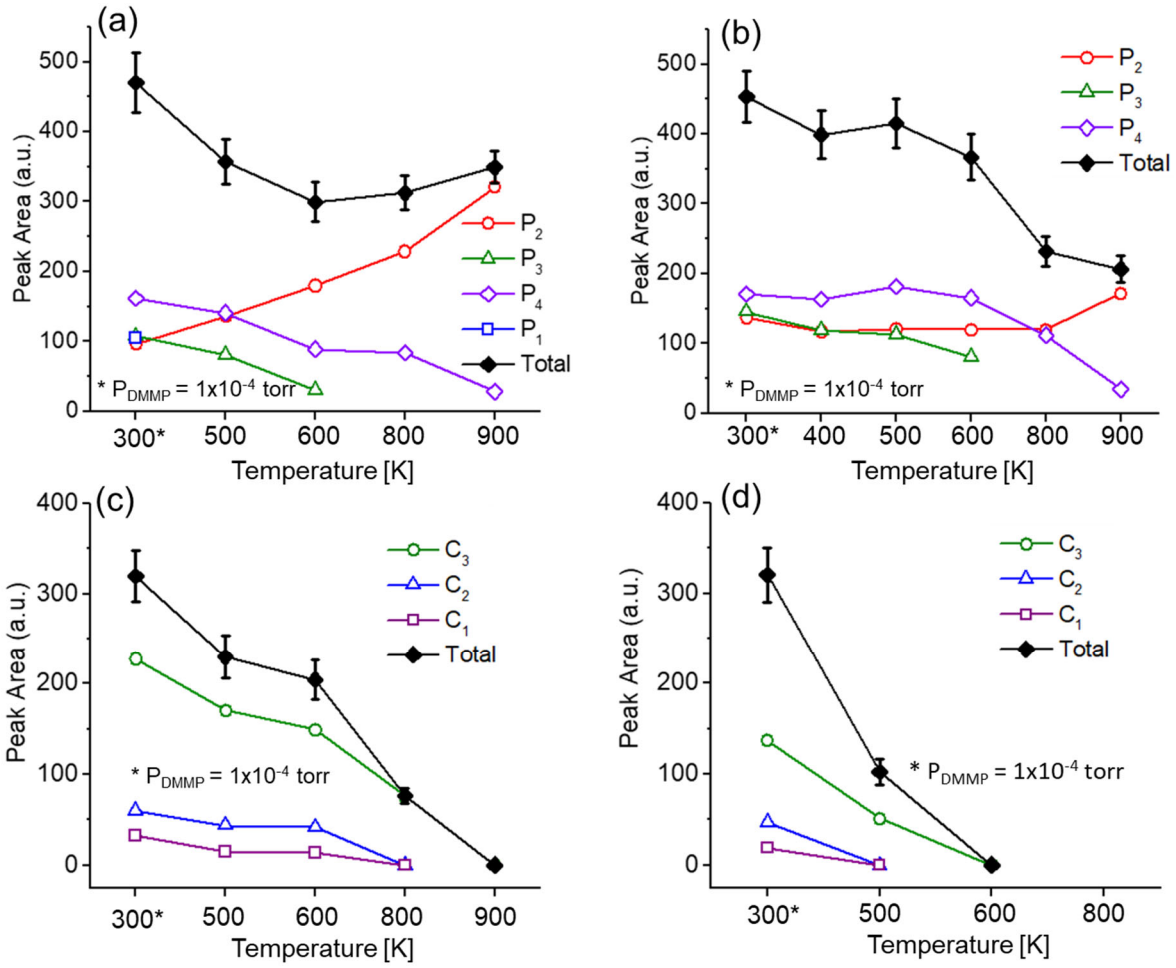

Figure 7: P 2p (a,b) and C 1s (c,d) peak intensities versus temperature for the (a, c) $Cu_4/TiO_2(110)$ and (b,d) $K/Cu_4/TiO_2(110)$ surfaces exposed $1x10^{-4}$ Torr of DMMP at room temperature. The DMMP was pumped out of the NAP-XPS chamber prior to heating the surfaces.

are given in SI, Figures S5, S6, and S7. On the Cu surface (Fig. 7a), the P_1, P_3 and P_4 species drop rapidly with increasing temperature with P_1 and P_3 undetectable above 400 K and 600 K, respectively. The loss of P_1 at low temperatures is consistent with the assignment to molecular DMMP which is known to desorb and decompose on TiO_2(110) above 400 K.[11-12,26] The P_4 species, assigned to atomic-P, is more stable with ~20% remaining on the surface at 900 K. By contrast, the P_2 peak intensity exhibits the opposite behavior and increases by more than 3x from RT to 900 K. These temperature trends suggest that P_3 and P_4 species are being oxidized and converted to P_2 at higher temperature. This conclusion is supported by the total surface concentration of P species, which drops when heated to 600 K to ~75% of its initial value at 900K where it is nearly equal to the P_2 signal.

The surface concentration of the reduced P_3 species on the K-Cu surface (Fig. 7b) follows a similar trend as the Cu only surface and is undetectable above 600 K. However, the trends for the surface concentrations of P_2, P_4 and total P are very different for the K-Cu surface as compared to the Cu only surface. Specifically, the concentrations of both P_2 and P_4 are essentially constant from RT to 600 K, while the drop in total P can be largely associated with the loss of P_3 species. Above 600 K, the P_4 species falls off rapidly to ~20% of its maximum value, while P_2 remains constant till 800 K and then increases at 900K (Fig. 7b). The drop in the total P intensity above 600K follows the sum of $P_2 + P_4$, and is nearly the same as P_2 at 900 K. Overall, the total P present on the K-Cu surface continuously drops with increasing temperature to only ~45% of its maximum value at 900 K as compared to 75% on the Cu surface. The temperature dependent results show that the presence of K atoms enhances stability of the highly reduced P_4 species, while also promoting the removal of P-containing decomposition products at temperatures > 600K.

Overall, the temperature trends in Figures 7a and 7b show that 25% and 55% of the initial P 2p signal on the Cu and K-Cu surfaces is lost after annealing to 900 K. For the Cu surface, the decrease in P 2p signal is attributed to a combination of DMMP desorption and the loss of the P_3 and P_4 species which are partly removed from the surface and partly converted to the more oxidized P_2 species which grows in intensity at higher annealing temperatures. On the K-Cu surface, for which molecular DMMP is not present, the drop in P 2p signal is evidently due to the loss of P_3 and P_4 as conversion to P_2 is only evident at 900 K. We assume that the loss of P_3 and P_4 from the Cu and K-Cu surfaces results from thermally induced decomposition and desorption of the fragments, e.g., PO, but we cannot rule out the possibility that the decrease in P 2p signal is associated with P atom diffusion into the bulk TiO_2 crystal. For DMMP decomposition on Pt(111)[54] and Pt nanoparticles (~42 nm dia., 0.5 ML coverage) supported on TiO_2(110),[11] the loss of surface P was attributed to P-atom diffusion into the bulk Pt crystal or the large Pt nanoparticles. According to the DFT calculations for the Cu and K-Cu surfaces studied here, the P_3 and P_4 species result from 2-3 bond cleavages of adsorbed DMMP which are bonded to the surface via P-O-Ti_{5c}, P-O_{br} and P-O-Cu bonds (see Figures 10-12). The P-O-Ti_{5c} and/or P-O_{br} linkages would likely anchor the P-atoms to the TiO_2 surface and thereby inhibit subsurface diffusion. Future studies using TPD and/or XPS/Auger depth profiling will be needed to further investigate whether P desorption or subsurface diffusion are responsible for loss of surface P on these surfaces at higher temperature.

The temperature trends in Figure 7a and 7b are similar to that observed for heating the Cu_2O surface to ~540 K after exposure to DMMP for which the P 2p peaks associated with more reduced P-species are converted to a single P-species at higher binding energy close to that of P_2.[22] Based on the P:O stoichiometry after heating, this species was attributed to P_2O_5. For bare

TiO_2(110) and Cu nanoparticles supported on TiO_2(110) that were exposed to a saturation coverage of DMMP, the P 2p peak near the P_2 binding energy after annealing to 850 K was also assigned to a PO_x species (see Table 1).[12,26] Based on these earlier studies, it is likely that the final product denoted as P_2 on the Cu and K-Cu surfaces after high temperature annealing is a PO_x species that is strongly bound to the TiO_2 surface. This assignment is consistent with conversion of more reduced P_3 and P_4 species to a more oxidized product as evidenced in Figure 7a and 7b.

The temperature dependence of the C 1s peak intensities after heating the Cu and K-Cu surfaces are shown in Figure 7c-d (the individual C 1s XPS spectra at 300 K, 500 K and 800 K for both surfaces are shown in SI, Figure S7). The primary difference between the Cu and K-Cu surfaces is that the initial concentrations of C-species associated with DMMP decomposition are higher on the K-Cu surface. On both surfaces, the peak intensities for C_1-C_3 decrease rapidly with increasing temperature and are mostly undetectable above 600 K. The exception is C_3 on the K-Cu surface, where its larger initial concentration extends its detectability to > 600 K. These results show that the Cu and K-Cu surfaces are mostly free of C-based intermediates resulting from DMMP decomposition after heating to 600-800 K (see Figures S7c and S7f in SI).

Figure 8a shows the effects of DMMP adsorption, decomposition and increasing surface temperature on the state of reduction of the TiO_2(110) support for the Cu and K-Cu surfaces (the individual Ti 2p XPS spectra with fits are given in SI, Figures S8). Without K, the fraction of Ti^{3+} is roughly unchanged (~4%) from the as-prepared surface (Fig. 1a) and increases above 600 K to about 8% at 900 K. Reduction of the TiO_2(110) surface is expected at temperatures > 600 K via the formation of bridged oxygen vacancies and associated reduced Ti^{3+}cations.[33] Interestingly, the K-Cu surface exposed to DMMP becomes more oxidized when heated from 300-600 K, i.e., the

Ti^{3+} percentage drops from 8% to 4%, followed by reduction at 800 K. The final state of reduction is the same for both surfaces at (~8%) at 900 K.

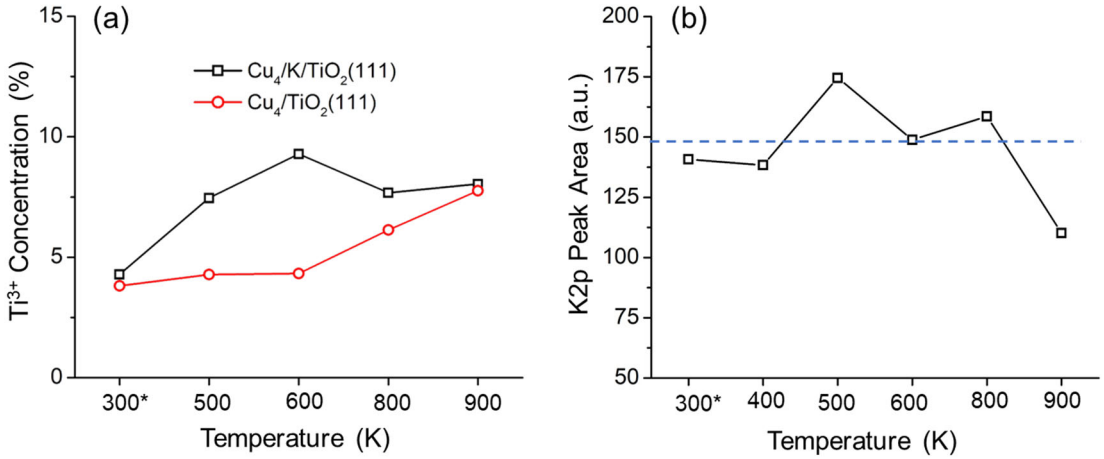

Figure 8: (a) The Ti^{3+} concentration as determined from fitting the Ti 2p XPS spectra at different temperatures for the $Cu_4/TiO_2(110)$ and $Cu_4/K/TiO_2(110)$ surfaces. (b) K 2p XPS peak intensity versus temperature for the $Cu_4/K/TiO_2(110)$ surface. The 300 K data points presented in (a) and (b) were taken under $1x10^{-4}$ Torr of DMMP, while DMMP was evacuated for measurements taken at higher temperatures.

The unusual temperature dependence observed for the Ti^{3+} concentration for the K-Cu surface is attributed to the surface coverage of K atoms, which can be probed by the K 2p XPS intensity. As shown in Figure 8b, the K coverage is roughly constant up to ~800 K, above which the K coverage decreases by about 30% via evaporation. The loss of K from the surface reduces electron donation to the TiO_2 support and thereby "oxidizes" the surface with a decrease in the number of reduced Ti^{3+} cations (Fig. 8a). We expect the bonding of P-intermediates to reduced Ti^{3+} cations to be weaker (lower Lewis acidity) compared to Ti^{4+} so that they can be more readily removed from the surface with increasing temperature. This may explain why the K-Cu surface generates a lower concentration of oxidized P_1 species at temperatures below 800 K where the K adatoms are stable (Fig. 8b). Moreover, the temperature dependence of highly reduced P_4 species

on the K-Cu surface (Fig. 7b) exhibits a similar profile as the K intensity (Fig. 8b) suggesting that K enhances the stability of the P_4 species.

IV. Discussion

Comparison of the XPS spectra for the Cu, K-Cu and K surfaces (Fig. 5), demonstrates that the presence of Cu_4 clusters is essential to DMMP decomposition, as no P-based fragments are observed for the K only surface. The presence of both K atoms and Cu_4 clusters on TiO_2(110) further enhances reactivity with only decomposition fragments and no molecular DMMP observed on the surface at RT. The K-Cu surface also improves the removal of the decomposition products at high temperatures. Although the Cu and K-Cu surfaces exhibit high activity for DMMP decomposition at RT, the peak intensities in the P 2p and C 1s XPS spectra do not continue to grow under constant DMMP exposure (at 1×10^{-4} Torr) suggesting that the surface is saturated with DMMP and/or intermediates resulting from DMMP decomposition. Moreover, the P and C intermediates could only be decreased by heating the surfaces above 500 K, with some PO_x species remaining even after heating to 900 K. These observations indicate that DMMP decomposition on the Cu and K-Cu surfaces at RT results in some strongly bound reaction products that block adsorption and reaction sites and, thereby, limit the number of turn-overs for DMMP decomposition. Moreover, the presence of some strongly bound PO_x species after high temperature heating, albeit at lower coverage on the K-Cu surface, prevents the surfaces from being fully regenerated at temperatures ≤ 900 K.

Comparing the results of this work with XPS experiments of DMMP decomposition on other related surfaces (see Table 1), we can make reasonable assignments of the fitted P 2p peaks to specific DMMP molecular fragments. Because the observed binding energies vary for different TiO_2 surfaces with different admetals, these assignments are tentative at best without other corroborating evidence such as IR vibrational spectra under the same experimental conditions.

Moreover, the complexity of the ternary K/Cu_4/TiO_2(110) system, where the decomposition fragments can bind at TiO_2, Cu_4, or K sites and their interfaces, could give rise to a much wider range of P 2p binding energies than on the surfaces of pure materials (e.g., Cu_2O) or a binary metal-on-oxide surfaces. Hence, it may be more appropriate to view the P 2p spectra as representing an overlapping distribution of chemical shifts corresponding to P atoms in many different local environments instead of assigning the incompletely resolved XPS spectra to a few specific decomposition products. Here, we used DFT calculations to sample a large number of energetically favorable decomposition configurations for DMMP on the Cu and K-Cu surfaces to better understand how the Cu_4 and K metals promote DMMP decomposition and how final state fragment distributions influence the chemical environment of the P-based fragments. The latter is reflected in the calculated P 2p chemical shifts (δ_{XPS}) and the resulting manifold of shifts can be compared to the experimental P 2p XPS spectra. Possible isomers of decomposed DMMP via the cleavage of one, two, or three O-C, P-O and P-C bonds on the Cu and K-Cu surfaces were exhaustively explored (290 configurations). The electronic adsorption energies of the different chemisorbed DMMP and their decomposition configurations relative to gas-phase DMMP on the Cu and K-Cu surfaces are plotted in Figure 9. On both surfaces, the Cu_4 clusters provide a very strong thermodynamic drive for full DMMP decomposition with many isomer configurations having energies lower than chemisorbed DMMP, up to 2 eV (~190 kJ/mol) lower. The isomer configuration energies are systematically larger in absolute value (more negative) for the Cu compared to the K-Cu surface suggesting that the presence of K atoms weakens interactions between the dissociation products and binding sites on the K/Cu_4/TiO_2(110). The latter is consistent with the observed temperature trends in Figure 7 where P-species resulting from DMMP decomposition are more easily removed from the K-Cu surface when heated above 600 K.

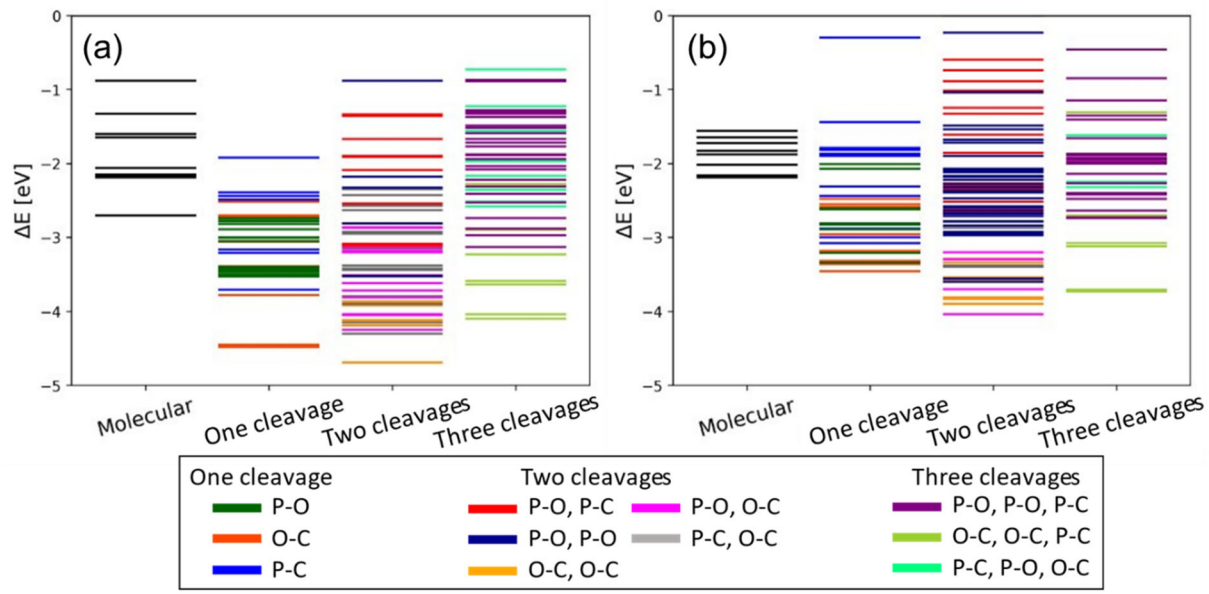

Figure 9: Computational exploration of DMMP decomposition intermediates, combining bond dissociation at the P atom (P-C or P-OCH_3 bond cleavage) and O-C bond dissociation on (a) $Cu_4/TiO_2(110)$ and (b) $K/Cu_4TiO_2(110)$ surfaces. "Molecular" indicates non-dissociated chemisorbed DMMP. The adsorption energies (ΔE) of each configuration are referenced to gas-phase DMMP.

Selected ensemble of configurations with low adsorption energy or interesting XPS binding shifts after breaking one, two, and three bonds in DMMP on Cu and K-Cu surfaces are shown in Figures 10 and 11, respectively. On the Cu surface, the most stable configurations resulting from 1-bond and 2-bond cleavages involve breaking O-C bonds to form CH_3 fragments, while 3-bond cleavages that release three CH_3 fragments by breaking two O-C and one P-C bonds are thermodynamically more favorable. The released CH_3 fragments bind predominantly to the Cu_4 clusters or more rarely to O-lattice atoms of the TiO_2 support. These most stable configurations therefore generate a large fraction of methyl groups bound to Cu, in complete agreement with the very low C2:C3 ratio of peaks in the C XPS spectra discussed above. The best two-bond cleavage configuration is slightly more favorable (δE_{rel} =-1.99 eV, δE_{rel} denotes the stability of an intermediate with respect to the chemisorbed DMMP) than the best one-bond configuration

(δE_{rel}= -1.75 eV), but the product of the 3-bond cleavage is somewhat less stable (δE_{rel}= -1.35 eV), although still markedly favored compared to intact chemisorbed DMMP on the TiO_2 surface.

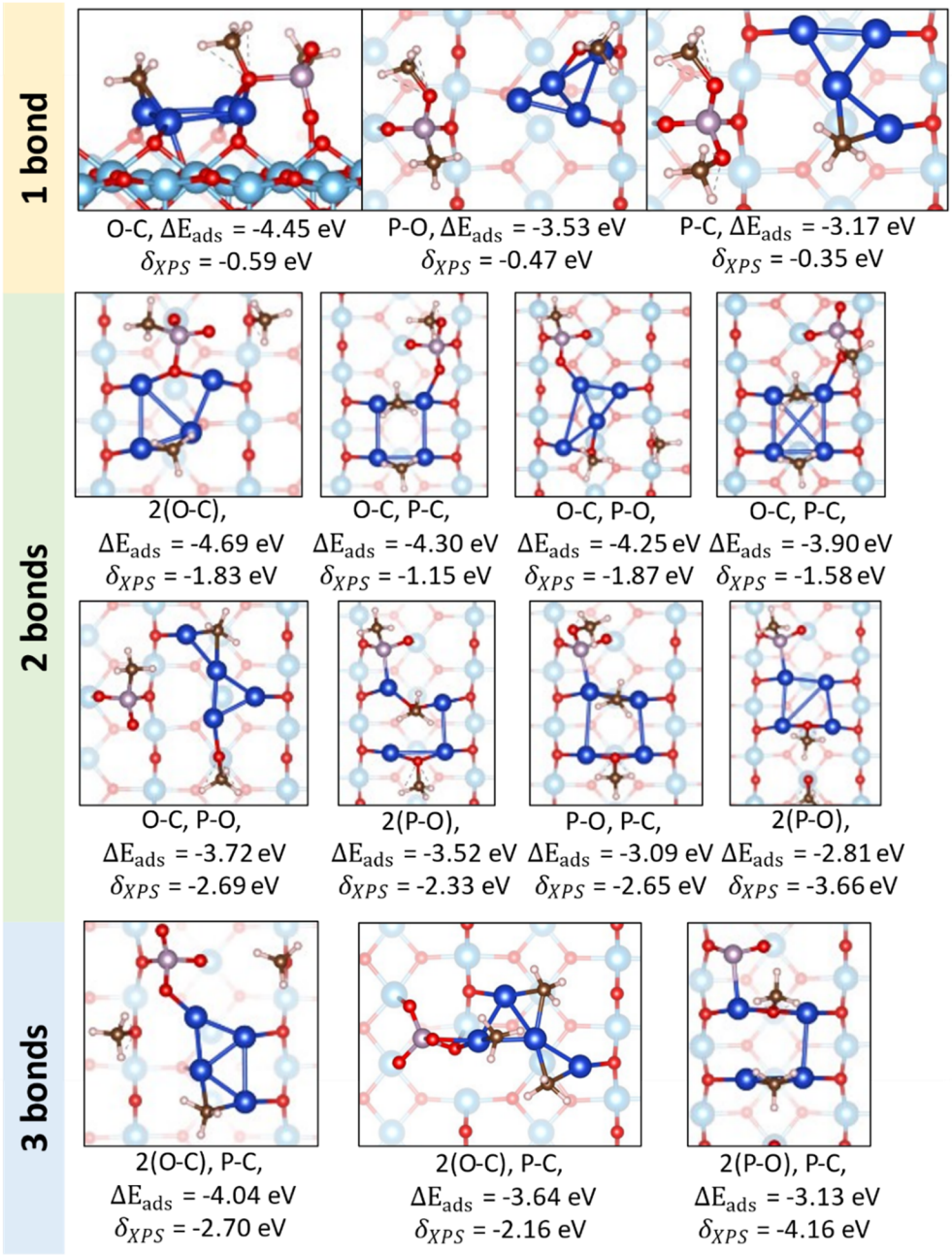

Figure 10: Surface structures for the most stable and unique P-center containing intermediates for DMMP decomposition on $Cu_4/TiO_2(110)$ along with their respective adsorption energies (ΔE_{ads} referenced to gas-phase DMMP) and XPS binding shifts (δ_{XPS}) for breaking one, two, and three bonds. Atom colors: Ti: light blue; O: red; Cu: dark blue; K: purple; P: silver; C; brown.

On the K-Cu surface, breaking only one O-C bond still results in the most stable 1-bond configuration (δE_{rel}= -1.27 eV), whereas the lowest energy configuration for breaking 2-bonds involves one O-C and one P-O bond (δE_{rel}= -1.85 eV), while the result of two O-C cleavages is close in energy (δE_{rel} =-1.71). Similar to the Cu surface, two O-C and one P-C bonds are broken

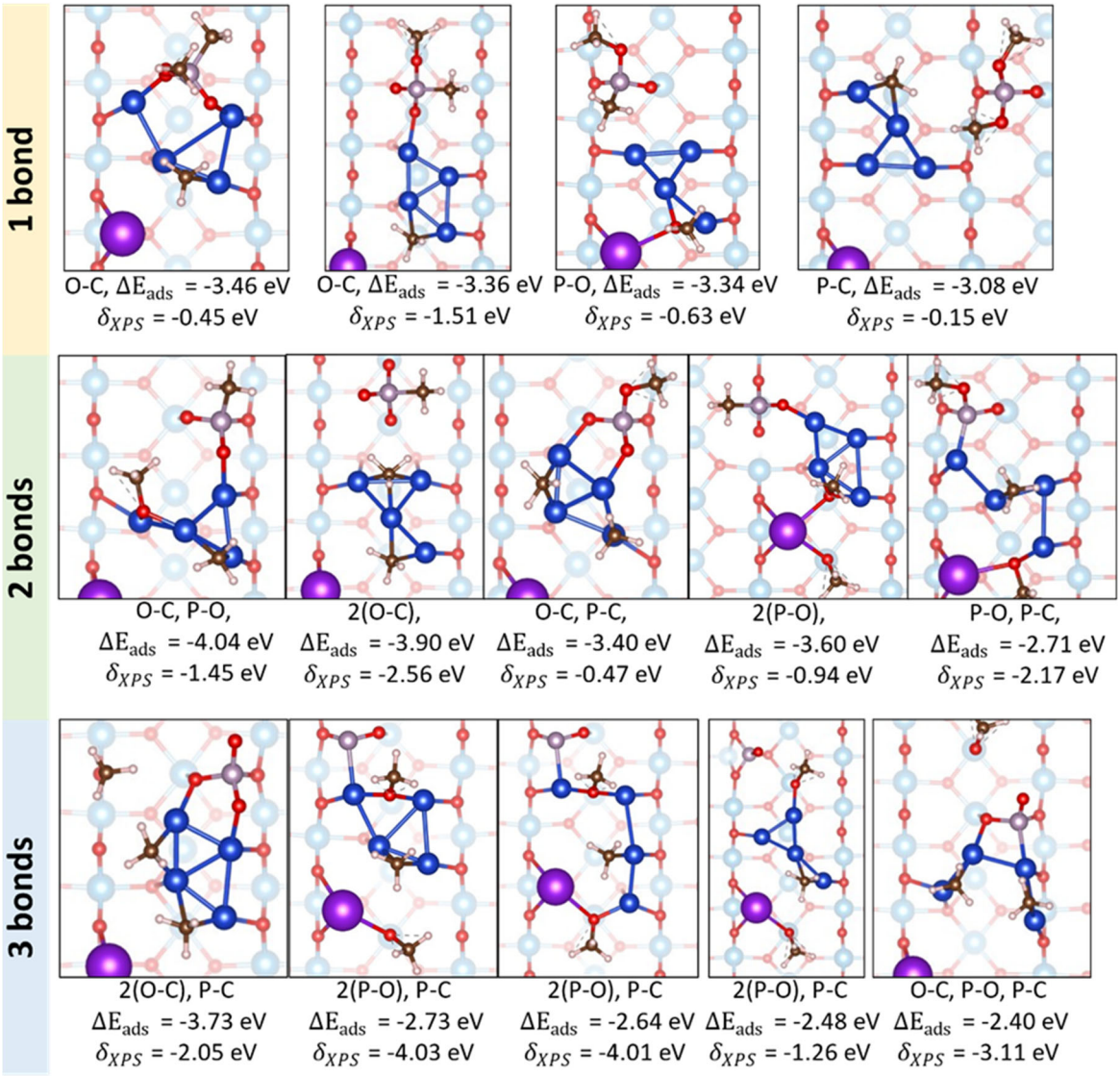

Figure 11: Surface structures for the low energy and unique intermediates for DMMP decomposition on K/Cu_4/TiO_2(110) along with their respective adsorption energies (ΔE_{ads} referenced to gas-phase DMMP) and XPS binding shifts (δ_{XPS}) for breaking one, two, and three bonds.). Atom colors: Ti: light blue; O: red; Cu: dark blue; K: purple; P: grey; C; brown.

in the lowest energy configuration for 3-bond cleavages (δE_{rel}= -1.53 eV). In all the configurations sampled, the CH_3O and CH_3 fragments are stabilized on the Cu_4 clusters, even in the presence of K atoms. Again, a large ratio of methyl bound to Cu are formed, in agreement with the C 1s spectra. The surface structures in Figures 10-11 also highlight the dynamic (fluxional) nature of Cu_4 clusters, with marked deformations of the Cu_4 cluster structure to accommodate the methyl or methoxy ligands, and the wide range of molecular fragment binding sites for the remaining P-moieties that determine the local chemical environment and, thereby, the 2p binding energies of these P-fragments.

In order to identify the P-fragments that are most likely to contribute to the XPS spectra, P 2p binding energy shifts (δ_{XPS}) were calculated and plotted as a function of the stability of the isomer configuration (Figure 12). Stability here is defined as the absolute value of the energy change with respect to chemisorbed DMMP, i.e.,

$$E_{stability} = |\delta E_{rel}| = |E_{isomer} - E_{chemisorbed\ DMMP}|$$

A more positive value hence means a more stable configuration. The calculated P 2p binding energy shifts for all the fragment configurations sampled on the Cu and K-Cu surfaces are shown in Figures 12a and 12e, respectively. The calculated shifts range from -1 to -4 eV, agreeing well with the experimental data (Figure 5). Moreover, the magnitude of the calculated shifts exhibits clear trends with (1) the number of bonds broken or fragments transferred to the surface and (2) the types of bonds cleaved. These trends are evident in Figures 12b-12d and 12f-12h, which separate the calculated shifts for fragment configurations resulting from 1-bond, 2-bond and 3-bond cleavages. Firstly, as the degree of decomposition increases, the binding energy shift increases. Secondly, for isomers resulting from 1-bond dissociations, the largest shifts are associated with O-C bond cleavage, followed by P-O and P-C bonds, although smaller shifts can

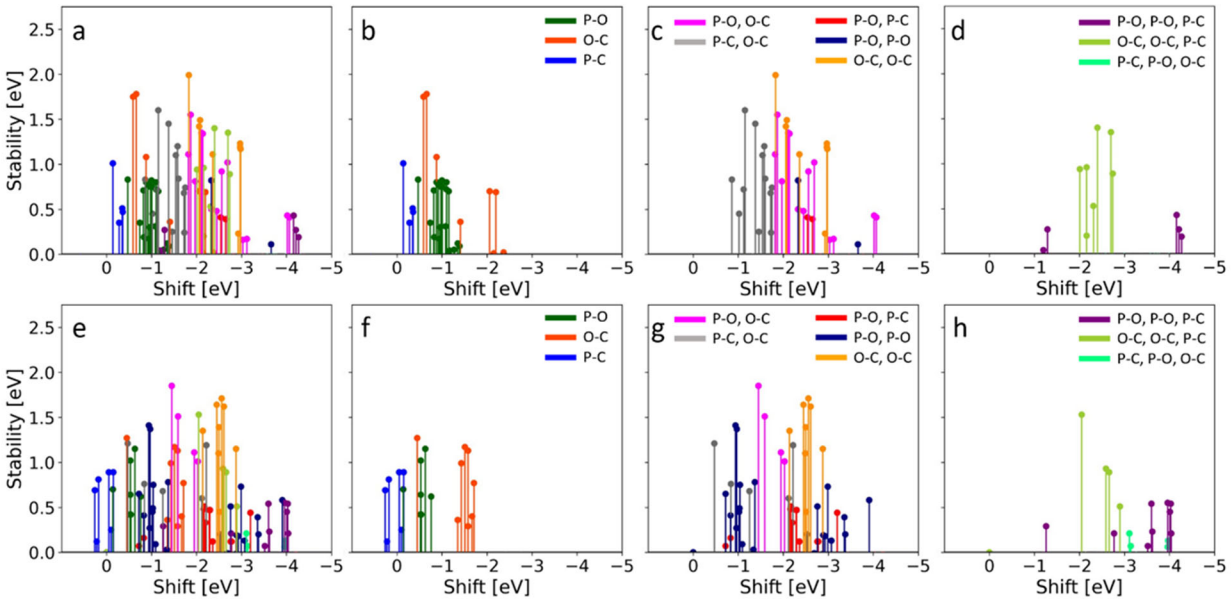

Figure 12: Calculated XPS binding energy shifts on P atom against its stability on Cu_4/TiO_2 (a-d) and KC_{u4}/TiO_2 (e-h) referenced to the molecularly chemisorbed DMMP. Plot b-d and f-h showcase the peaks obtained from isomers with one, two and three fragment transferred onto Cu4 and Cu4K clusters respectively. The label P-O, P-C and O-C denotes which bonds/combination of bonds are broken (P-O, P-C and O-C bonds respectively).

also be seen for a few intermediates with O-C bond cleavage (Fig. 12b). For 2-bond dissociations, isomers with a P center that possesses either phosphoryl groups (P=O) resulting from O-C bond cleavage or that underwent P-O bond cleavage generally have larger shifts. Isomer configurations with fully reduced P centers, where all the P-O and P-C bonds are cleaved, have the largest calculated shifts, close to -4 eV. These P centers re-coordinate with Cu atoms and a few surface O atoms for their stability. Correlations between the calculated P 2p binding energy shifts and the oxidation state of the P center as inferred from Bader charge analyses are shown in Figures S9 and S10 for the Cu and K-Cu surfaces, respectively. The latter show that as the degree of decomposition increases, the Bader charge on the P atom decreases, i.e., it becomes more reduced, and the binding energy shifts to lower energies.

Overall, the calculated trends in Figures 12, S9 and S10 are in qualitative agreement with previous studies of DMMP decomposition where negative P 2p binding shifts (relative to intact DMMP) were attributed to fragments with fewer bonds to the P center, with atomic P species exhibiting largest shift (see Table 1). Here, we identified the P_2 peaks with a shift of about -1 eV (w.r.t. to P_1, chemisorbed DMMP) to methyl methylphosphonate (MMP). This assignment is consistent with the calculated 1-bond shifts for O-C bond cleavage on Cu and K-Cu surfaces (Fig.s 12b and 12f); however, binding energy shifts near -1 eV can also include contributions from P-species resulting from 2-bond breaking processes (O-C and P-O) with similar energy stabilities (Fig.s 12c and 12g). Similarly, the P_3 peaks with observed shifts near -3.2 eV are likely to be a mix of P-species resulting from multiple 2-bond dissociations (Fig. 12c and 12g) on both surfaces, although configurations resulting from two O-C cleavages have the highest calculated stability. Finally, the calculations suggest that the P_4 peaks exhibiting the largest calculated (-4 eV) and observed (-5.2 eV) binding energy shifts are likely associated with P-species resulting from 3-bond dissociation processes, i.e., two P-O and one P-C or two O-C and one P-O bond cleavages (Fig.s 12d and 12h). The P 2p peaks observed in this binding energy range on other surfaces such as those listed in Table 1 are typically assigned to "atomic P." The lowest energy structures in Figures 11 and 12 show that the most reduced species is a P-atom bonded to two O-atoms and the Cu_4 cluster on the Cu and K-Cu surfaces. Overall, the calculations show that the apparent peaks in the experimental P 2p spectra (Figure 5) are not likely associated with any specific DMMP fragment. Instead, the XPS spectra are better described by a manifold of P-atom chemical environments that depend sensitively on the final state configuration of fragments on the surface and the number and type of bonds broken (Fig.s 10-12).

As demonstrated in this work, the use of mass-selected cluster deposition is well suited for exploring the reactivity of ultra-small clusters, but the cluster throughput is too small for generating macroscopic amounts of materials. Conventional bench-top catalysis synthesis method, e.g., wet impregnation or co-precipitation, are scalable and the synthesis of materials composed of Cu nanoparticles (sizes ≥ 1.5 nm) with K dopants supported on high surface area titania is relatively straightforward using common Cu and K precursors.[55] The preparation of sub-nm or Cu clusters with 10's of atoms is significantly more challenging but has been demonstrated for oxide supported Cu single atom and ultra-small Cu clusters via thermal diffusion,[56] confinement in zeolite pore structures,[57-58] electrochemical dissolution[59] and dendritic encapsulation.[60] As new synthesis methods develop, it should be possible to prepare K/Cu/TiO_2 powders analogous to the model systems used in this work and test them under exposure to DMMP or actual CWA's in flow or sealed reactors.

V. Conclusions

In this work, NAP-XPS combined with DFT calculations were used to probe the reactivity of the TiO_2(110) surface modified with the deposition of ultra-small Cu_4 clusters and alkali metal (K) atoms for the decomposition of a CWA simulant, DMMP. By itself, TiO_2(110) is inactive for DMMP decomposition except at elevated temperatures. By contrast, the Cu_4/TiO_2(110) surface is found to be very reactive, with highly reduced P-species observed even at RT. The co-deposition of K atoms further enhances the reactivity and also improves the removal of the decomposition products at high temperatures. The P 2p and C 1s core level spectra, and our DFT calculations, indicate that DMMP decomposition on Cu and K-Cu surfaces involves cleavage of P-O, P-C and C-O bonds to form chemisorbed methoxy and methyl groups on the surface. Using comparisons with previous studies of DMMP decomposition on other related surfaces, the incompletely

resolved peaks in the P 2p spectra could be tentatively assigned to specific P-based species, including DMMP, MMP and "atomic" P. To gain a more atomistic picture of the decomposition pathways that lead to the observed decomposition products, detailed ab initio DFT calculation were performed to determine the surface distribution of decomposition products for a large number of energetically favorable final state configurations (290) resulting from 1-3 bond cleavages in chemisorbed DMMP. The calculations show that intact DMMP preferentially binds to the TiO_2(110) surface, although the binding energy is sensitive to the presence of nearby Cu_4 clusters and K atoms. Moreover, the calculations show that the Cu_4 clusters strongly promote P-O, O-C and P-C bond cleavage in DMMP and are highly fluxional with atomic structures that depend on the configuration of fragments bound to the surface. For each configuration of final state decomposition products, the P 2p binding energy shift relative to chemisorbed DMMP was calculated. The predicted energy shifts range from -1 to -4 eV, which is in reasonable agreement with the energy widths of the experimental P 2p spectra. The magnitudes of the calculated shifts depend on the number of bonds broken and which type of bond is cleaved, e.g., P-O or P-C. The largest shifts are associated with P centers where all three P-O and P-C bonds are cleaved and that re-coordinate to Cu at surface O atoms ("atomic" P species). This suggests that the broad P 2p core level spectra are better described by a near continuous distribution of P 2p chemical shifts that arise from the large number of energetically accessible decomposition configurations. When only a few final state configurations are energetically favorable, this analysis leads to similar conclusions as the conventional peak fitting approach, where each peak can be "assigned" to a different oxidation state. More broadly, this combined experimental and computational study sheds new light on the interpretation of core level spectra associated with intermediates resulting from complex surface reactions.

Acknowledgements

The authors gratefully acknowledge Dr. Ashley Head, Jason Wang and Luolin Shi for their help in setting up and running experiments at the Center for Functional Nanomaterials. MB, MW, CT, PS acknowledge support from the U.S. Army Research Laboratory and the U.S. Army Research Office under Grant No. W911NF-20-2-0058 (MB, MW) and W911NF-21-1-0361 (CT, PS). The views and conclusions herein are those of the authors and should not be interpreted as necessarily representing the official policies or endorsements, either expressed or implied, of the ARO or the U.S. Government. The NAP-XPS measurements were performed at the Center for Functional Nanomaterials, a U.S. DOE Office of Science User Facility located at Brookhaven National Laboratory. This work used computational and storage services associated with the Hoffman2 Shared Cluster provided by UCLA Office of Advanced Research Computing's Research Technology Group. This work used Bridges-2 at Pittsburgh Supercomputing Center through allocation CHE170060 from the Advanced Cyberinfrastructure Coordination Ecosystem: Services & Support (ACCESS) program, which is supported by National Science Foundation grants #2138259, #2138286, #2138307, #2137603, and #2138296.[61]

Conflict of Interest: The authors have no known conflict of interests concerning the publication of this research.

SI Content

Cu LMM Auger spectra for different conditions; P 2p, C 1s and Ti 2p XPS spectra at different temperatures; calculated Bader charges versus P 2p binding energy shifts

References Cited

1. Nawała, J.; Jóźwik, P.; Popiel, S., Thermal and Catalytic Methods Used for Destruction of Chemical Warfare Agents. *Inter. J. Environ. Sci. Technol.* **2019**, *16*, 3899-3912.

2. Kim, K.; Tsay, O. G.; Atwood, D. A.; Churchill, D. G., Destruction and Detection of Chemical Warfare Agents. *Chem. Rev.* **2011**, *111*, 5345-5403.

3. Mukhopadhyay, S.; Schoenitz, M.; Dreizin, E. L., Vapor-Phase Decomposition of Dimethyl Methylphosphonate (Dmmp), a Sarin Surrogate, in Presence of Metal Oxides. *Def. Technol.* **2020**, *17*, 1095-1114.

4. Mitchell, M. B.; Sheinker, V. N.; Mintz, E. A., Adsorption and Decomposition of Dimethyl Methylphosphonate on Metal Oxides. *J. Phys. Chem. B* **1997**, *101*, 11192-11203.

5. Cao, L. X.; Segal, S. R.; Suib, S. L.; Tang, X.; Satyapal, S., Thermocatalytic Oxidation of Dimethyl Methylphosphonate on Supported Metal Oxides. *J. Catal.* **2000**, *194*, 61-70.

6. Sheinker, V. N.; Mitchell, M. B., Quantitative Study of the Decomposition of Dimethyl Methylphosphonate (Dmmp) on Metal Oxides at Room Temperature and Above. *Chem. Mat.* **2002**, *14*, 1257-1268.

7. Vellingiri, K.; Philip, L.; Kim, K. H., Metal-Organic Frameworks as Media for the Catalytic Degradation of Chemical Warfare Agents. *Coord. Chem. Rev.* **2017**, *353*, 159-179.

8. Grissom, T. G.; Plonka, A. M.; Sharp, C. H.; Ebrahim, A. M.; Tian, Y. Y.; Collins-Wildman, D. L.; Kaledin, A. L.; Siegal, H. J.; Troya, D.; Hill, C. L.; Frenkel, A. I.; Musaev, D. G.; Gordon, W. O.; Karwacki, C. J.; Mitchell, M. B.; Morris, J. R., Metal-Organic Framework- and Polyoxometalate-Based Sorbents for the Uptake and Destruction of Chemical Warfare Agents. *ACS Appl. Mater. Interfaces* **2020**, *12*, 14641-14661.

9. Trubitsyn, D. A.; Vorontsov, A. V., Experimental Study of Dimethyl Methylphosphonate Decomposition over Anatase Tio2. *J. Phys. Chem. B* **2005**, *109*, 21884-21892.

10. Moss, J. A.; Szczepankiewicz, S. H.; Park, E.; Hoffmann, M. R., Adsorption and Photodegradation of Dimethyl Methylphosphonate Vapor at Tio2 Surfaces. *J. Phys. Chem. B* **2005**, *109*, 19779-19785.

11. Ratliff, J. S.; Tenney, S. A.; Hu, X.; Conner, S. F.; Ma, S.; Chen, D. A., Decomposition of Dimethyl Methylphosphonate on Pt, Au, and Au−Pt Clusters Supported on Tio2(110). *Langmuir* **2009**, *25*, 216-225.

12. Ma, S.; Zhou, J.; Kang, Y. C.; Reddic, J. E.; Chen, D. A., Dimethyl Methylphosphonate Decomposition on Cu Surfaces: Supported Cu Nanoclusters and Films on Tio2(110). *Langmuir* **2004**, *20*, 9686-9694.

13. Panayotov, D. A.; Morris, J. R., Catalytic Degradation of a Chemical Warfare Agent Simulant: Reaction Mechanisms on Tio2-Supported Au Nanoparticles. *J. Phys. Chem. C* **2008**, *112*, 7496-7502.

14. Tzou, T. Z.; Weller, S. W., Catalytic-Oxidation of Dimethyl Methylphosphonate. *J. Catal.* **1994**, *146*, 370-374.

15. McEntee, M.; Gordon, W. O.; Balboa, A.; Delia, D. J.; Pitman, C. L.; Pennington, A. M.; Rolison, D. R.; Pietron, J. J.; DeSario, P. A., Mesoporous Copper Nanoparticle/Tio2 Aerogels for Room-Temperature Hydrolytic Decomposition of the Chemical Warfare Simulant Dimethyl Methylphosphonate. *ACS Appl. Nano Mat.* **2020**, *3*, 3503-3512.

16. Zhou, J.; Ma, S.; Kang, Y. C.; Chen, D. A., Dimethyl Methylphosphonate Decomposition on Titania-Supported Ni Clusters and Films: A Comparison of Chemical Activity on Different Ni Surfaces. *J. Phys. Chem. B* **2004**, *108*, 11633-11644.

17. Pillay, D.; Hwang, G. S., Structure of Small Aun, Agn, and Cun Clusters (N=2−4) on Rutile Tio2(110): A Density Functional Theory Study. *J. Mol. Struct.: Theochem* **2006**, *771*, 129-133.

18. Tao, H.; Li, Y.; Cai, X.; Zhou, H.; Li, Y.; Lin, W.; Huang, S.; Ding, K.; Chen, W.; Zhang, Y., What Is the Best Size of Subnanometer Copper Clusters for Co2 Conversion to Methanol at Cu/Tio2 Interfaces? A Density Functional Theory Study. *J. Phys. Chem. C* **2019**, *123*, 24118-24132.

19. Iyemperumal, S. K.; Fenton, T. G.; Gillingham, S. L.; Carl, A. D.; Grimm, R. L.; Li, G.; Deskins, N. A., The Stability and Oxidation of Supported Atomic-Size Cu Catalysts in Reactive Environments. *J. Chem. Phys.* **2019**, *151*.

20. Wang, R.-Y.; Wang, J.-X.; Jia, J.; Wu, H.-S., The Growth Pattern and Electronic Structures of Cun(N = 1–14) Clusters on Rutile Tio2(110) Surface. *App. Surf. Sci.* **2021**, *536*, 147793.

21. Trotochaud, L.; Tsyshevsky, R.; Holdren, S.; Fears, K.; Head, A. R.; Yu, Y.; Karslıoğlu, O.; Pletincx, S.; Eichhorn, B.; Owrutsky, J.; Long, J.; Zachariah, M.; Kuklja, M. M.; Bluhm, H., Spectroscopic and Computational Investigation of Room-Temperature Decomposition of a Chemical Warfare Agent Simulant on Polycrystalline Cupric Oxide. *Chem. Mat.* **2017**, *29*, 7483-7496.

22. Trotochaud, L.; Head, A. R.; Büchner, C.; Yu, Y.; Karslıoğlu, O.; Tsyshevsky, R.; Holdren, S.; Eichhorn, B.; Kuklja, M. M.; Bluhm, H., Room Temperature Decomposition of Dimethyl Methylphosphonate on Cuprous Oxide Yields Atomic Phosphorus. *Surf. Sci.* **2019**, *680*, 75-87.

23. Wang, L.; Denchy, M.; Blando, N.; Hansen, L.; Bilik, B.; Tang, X.; Hicks, Z.; Bowen, K. H., Thermal Decomposition of Dimethyl Methylphosphonate on Size-Selected Clusters: A Comparative Study between Copper Metal and Cupric Oxide Clusters. *J. Phys. Chem. C* **2021**, *125*, 11348-11358.

24. Rusu, C. N.; Yates, J. T., Adsorption and Decomposition of Dimethyl Methylphosphonate on Tio2. *J. Phys. Chem. B* **2000**, *104*, 12292-12298.

25. Kim, C. S.; Lad, R. J.; Tripp, C. P., Interaction of Organophosphorous Compounds with Tio2 and Wo3 Surfaces Probed by Vibrational Spectroscopy. *Sensors Actuators B: Chem.* **2001**, *76*, 442-448.

26. Zhou, J.; Varazo, K.; Reddic, J. E.; Myrick, M. L.; Chen, D. A., Decomposition of Dimethyl Methylphosphonate on Tio2(110): Principal Component Analysis Applied to X-Ray Photoelectron Spectroscopy. *Analyt. Chim. Acta* **2003**, *496*, 289-300.

27. Panayotov, D. A.; Morris, J. R., Uptake of a Chemical Warfare Agent Simulant (Dmmp) on Tio2: Reactive Adsorption and Active Site Poisoning. *Langmuir* **2009**, *25*, 3652-3658.

28. Panayotov, D. A.; Morris, J. R., Thermal Decomposition of a Chemical Warfare Agent Simulant (Dmmp) on Tio2: Adsorbate Reactions with Lattice Oxygen as Studied by Infrared Spectroscopy. *J. Phys. Chem. C* **2009**, *113*, 15684-15691.

29. Tesvara, C.; Walenta, C.; Sautet, P., Oxidative Decomposition of Dimethyl Methylphosphonate on Rutile Tio2(110): The Role of Oxygen Vacancies. *Phys. Chem. Chem. Phys.* **2022**, *24*, 23402-23419.

30. Hardman, P. J.; Casanova, R.; Prabhakaran, K.; Muryn, C. A.; Wincott, P. L.; Thornton, G., Electronic Structure Effects of Potassium Adsorption on Tio2(100). *Surf. Sci.* **1992**, *269-270*, 677-681.

31. Heise, R.; Courths, R., A Photoemission Investigation of the Adsorption of Potassium on Perfect and Defective Tio2(110) Surfaces. *Surf. Sci.* **1995**, *331-333*, 1460-1466.

32. Grant, A. W.; Campbell, C. T., Cesium Adsorption on Tio2(110). *Phys. Rev. B* **1997**, *55*, 1844-1851.

33. Diebold, U., The Surface Science of Titanium Dioxide. *Surf. Sci. Rep.* **2003**, *48*, 53-229.

34. An, W.; Xu, F.; Stacchiola, D.; Liu, P., Potassium-Induced Effect on the Structure and Chemical Activity of the Cuxo/Cu(1 1 1) (X ≤ 2) Surface: A Combined Scanning Tunneling Microscopy and Density Functional Theory Study. *ChemCatChem* **2015**, *7*, 3865-3872.

35. Chen, K. D.; Xie, S. B.; Bell, A. T.; Iglesia, E., Alkali Effects on Molybdenum Oxide Catalysts for the Oxidative Dehydrogenation of Propane. *J. Catal.* **2000**, *195*, 244-252.

36. Metiu, H.; Chrétien, S.; Hu, Z.; Li, B.; Sun, X., Chemistry of Lewis Acid–Base Pairs on Oxide Surfaces. *J. Phys. Chem. C* **2012**, *116*, 10439-10450.

37. Grinter, D. C.; R. Remesal, E.; Luo, S.; Evans, J.; Senanayake, S. D.; Stacchiola, D. J.; Graciani, J.; Fernández Sanz, J.; Rodriguez, J. A., Potassium and Water Coadsorption on Tio2(110): Oh-Induced Anchoring of Potassium and the Generation of Single-Site Catalysts. *J. Phys. Chem. Lett.* **2016**, *7*, 3866-3872.

38. Rodriguez, J. A.; Grinter, D. C.; Ramírez, P. J.; Stacchiola, D. J.; Senanayake, S., High Activity of Au/K/Tio2(110) for Co Oxidation: Alkali-Metal-Enhanced Dispersion of Au and Bonding of Co. *J. Phys. Chem. C* **2018**, *122*, 4324-4330.

39. Rodriguez, J. A.; Remesal, E. R.; Ramírez, P. J.; Orozco, I.; Liu, Z.; Graciani, J.; Senanayake, S. D.; Sanz, J. F., Water–Gas Shift Reaction on K/Cu(111) and Cu/K/Tio2(110) Surfaces: Alkali Promotion of Water Dissociation and Production of H2. *ACS Catal.* **2019**, *9*, 10751-10760.

40. Zhou, P.; Yu, J. G.; Nie, L. H.; Jaroniec, M., Dual-Dehydrogenation-Promoted Catalytic Oxidation of Formaldehyde on Alkali-Treated Pt Clusters at Room Temperature. *J. Mat. Chem. A* **2015**, *3*, 10432-10438.

41. Li, C. B.; Sivaranjani, K.; Kim, J. M., Synthesis of Alkali Promoted Mesoporous, Nanocrystalline Pd/Tio2 Catalyst for Water Gas Shift Reaction. *Catal. Today* **2016**, *265*, 45-51.

42. Li, Y. B.; Chen, X. Y.; Wang, C. Y.; Zhang, C. B.; He, H., Sodium Enhances Ir/Tio2 Activity for Catalytic Oxidation of Formaldehyde at Ambient Temperature. *ACS Catal.* **2018**, *8*, 11377-11385.

43. Yang, M.; Flytzani-Stephanopoulos, M., Design of Single-Atom Metal Catalysts on Various Supports for the Low-Temperature Water-Gas Shift Reaction. *Catal. Today* **2017**, *298*, 216-225.

44. Henderson, M. A.; Epling, W. S.; Perkins, C. L.; Peden, C. H. F.; Diebold, U., Interaction of Molecular Oxygen with the Vacuum-Annealed Tio2(110) Surface: Molecular and Dissociative Channels. *J. Phys. Chem. B* **1999**, *103*, 5328-5337.

45. Epling, W. S.; Peden, C. H. F.; Henderson, M. A.; Diebold, U., Evidence for Oxygen Adatoms on Tio2(110) Resulting from O2 Dissociation at Vacancy Sites. *Surf. Sci.* **1998**, *412-413*, 333-343.

46. Petrik, N. G.; Zhang, Z.; Du, Y.; Dohnálek, Z.; Lyubinetsky, I.; Kimmel, G. A., Chemical Reactivity of Reduced Tio2(110): The Dominant Role of Surface Defects in Oxygen Chemisorption. *J. Phys. Chem. C* **2009**, *113*, 12407-12411.

47. Sullivan, J. L.; Saied, S. O.; Bertoti, I., Effect of Ion and Neutral Sputtering on Single Crystal Tio2. *Vacuum* **1991**, *42*, 1203-1208.

48. Wagner, C. D.; Davis, L. E.; Zeller, M. V.; Taylor, J. A.; Raymond, R. H.; Gale, L. H., Empirical Atomic Sensitivity Factors for Quantitative Analysis by Electron Spectroscopy for Chemical Analysis. *Surf. Interface Anal.* **1981**, *3*, 211-225.

49. Huang, H. H.; Jiang, X.; Siew, H. L.; Chin, W. S.; Xu, G. Q., Water Dissociation and Koh Formation on Potassium-Covered Mgo/Ru(001). *Langmuir* **1998**, *14*, 7217-7221.

50. Biesinger, M. C., Advanced Analysis of Copper X-Ray Photoelectron Spectra. *Surf. Interface Anal.* **2017**, *49*, 1325-1334.

51. Tesvara, C.; Karwacki, C. J.; Sautet, P., Decomposition of the Toxic Nerve Agent Sarin on Oxygen Vacancy Sites of Rutile Tio2(110). *J. Phys. Chem. C* **2023**, *127*, 8006-8015.

52. Moulder, J. F.; Stickle, W. F.; Sobol, P. E.; Bomben, K. D., *Handbook of X-Ray Photoelectron Spectroscopy*; Perkin-Elmer Corp.: Eden Prairie, MN, 1992.

53. Zhou, J.; Ma, S.; Kang, Y. C.; Chen, D. A., Dimethyl Methylphosphonate Decomposition on Titania-Supported Ni Clusters and Films: A Comparison of Chemical Activity on Different Ni Surfaces. *J. Phys. Chem. B* **2004**, *108*, 11633-11644.

54. Henderson, M. A.; White, J., Adsorption and Decomposition of Dimethyl Methylphosphonate on Platinum (111). *J. Amer. Chem. Soc.* **1988**, *110*, 6939-6947.

55. Gawande, M. B.; Goswami, A.; Felpin, F.-X.; Asefa, T.; Huang, X.; Silva, R.; Zou, X.; Zboril, R.; Varma, R. S., Cu and Cu-Based Nanoparticles: Synthesis and Applications in Catalysis. *Chem. Rev.* **2016**, *116*, 3722-3811.

56. Yang, P.; Xu, J.; Tan, W.; Liu, Q.; Cai, Y.; Xie, S.; Hong, S.; Gao, F.; Liu, F.; Dong, L., Regulating the Pt1–Ceo2 Interaction Via Alkali Modification for Boosting the Catalytic Performance of Single-Atom Catalysts. *Chem. Commun.* **2023**, *59*, 6219-6222.

57. Grundner, S.; Markovits, M. A. C.; Li, G.; Tromp, M.; Pidko, E. A.; Hensen, E. J. M.; Jentys, A.; Sanchez-Sanchez, M.; Lercher, J. A., Single-Site Trinuclear Copper Oxygen Clusters in Mordenite for Selective Conversion of Methane to Methanol. *Nat. Commun.* **2015**, *6*, 7546.

58. Newton, M. A.; Knorpp, A. J.; Sushkevich, V. L.; Palagin, D.; van Bokhoven, J. A., Active Sites and Mechanisms in the Direct Conversion of Methane to Methanol Using Cu in Zeolitic Hosts: A Critical Examination. *Chem. Soc. Rev.* **2020**, *49*, 1449-1486.

59. Concepción, P.; Boronat, M.; García-García, S.; Fernández, E.; Corma, A., Enhanced Stability of Cu Clusters of Low Atomicity against Oxidation. Effect on the Catalytic Redox Process. *ACS Catal.* **2017**, *7*, 3560-3568.

60. Sonobe, K.; Tanabe, M.; Yamamoto, K., Enhanced Catalytic Performance of Subnano Copper Oxide Particles. *ACS Nano* **2020**, *14*, 1804-1810.

61. Boerner, T. J.; Deems, S.; Furlani, T. R.; Knuth, S. L.; Towns, J., Access: Advancing Innovation: Nsf's Advanced Cyberinfrastructure Coordination Ecosystem: Services & Support. In *Practice and Experience in Advanced Research Computing*, Association for Computing Machinery: Portland, OR, USA, 2023, pp 173–176.